

**PREPARATION AND INCORPORATION OF MULTI-FUNCTIONAL CARBON  
NANO MATERIALS INTO FIBER REINFORCED POLYMERIC COMPOSITES**

**by**

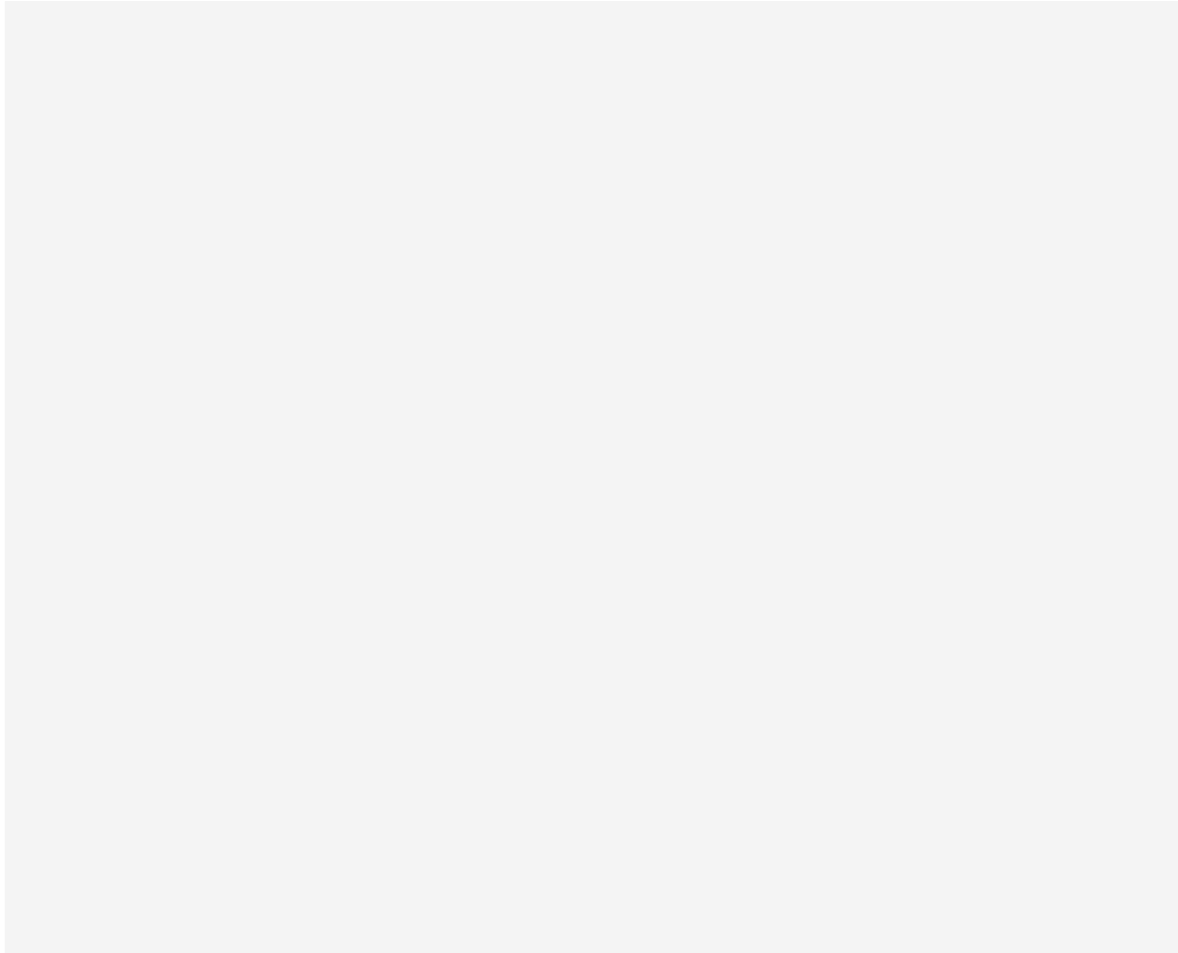
**Necdet Özçelik**

**Submitted to the Graduate School of Engineering and Natural Sciences  
in partial fulfilment of the requirements for the degree of  
Master of Science**

**Sabanci University  
July 2021**

PREPARATION and INCORPORATION OF MULTI-FUNCTIONAL  
CARBON NANO MATERIALS INTO FIBER REINFORCED POLYMERIC  
COMPOSITES

APPROVED BY:



DATE OF APPROVAL: 14.07.2021

**© Necdet Özçelik 2021**

**All Rights Reserved**

## **ABSTRACT**

### **PREPARATION AND INCORPORATION OF MULTI-FUNCTIONAL CARBON NANO MATERIALS INTO FIBER REINFORCED POLYMERIC COMPOSITES**

NECDET ÖZÇELİK

Materials Science and Nano Engineering M.Sc. Thesis, July 2021

Thesis Supervisor: Assist. Prof. Serkan Ünal

Keywords: Carbon Nanotubes, Glass Fiber Reinforced Polymeric Composites, Vacuum Infusion Process, Fiber-Matrix Interface, Ultrasonic Spray Deposition

It is well established that the use of nanomaterials as one of the components of fiber reinforced polymeric composite (FRPC) materials can significantly improve their mechanical, thermal, and electrical properties. The type of such nano-scale reinforcements and the processes for their incorporation into FRPCs are expected to be both cost effective and industrially feasible to enable their applications in various sectors, such as aerospace, aviation, military, and automotive, where high-performance materials are demanded. An effective incorporation and uniform distribution of nanomaterials at the interface between the polymer matrix and the fiber, which is one of the most complex regions in an FRPC structure, might enable a more efficient load transfer from the matrix to the fiber. However, to achieve significant improvements systematically, key problems associated with carbon nanomaterials such as undesired agglomeration, dispersion difficulties, and inability to provide functionality on the surface need

to be addressed properly. In this study a novel multi-functional silane coupling agent (SEPPS) was designed and synthesized for the incorporation of single-walled carbon nanotubes (SWCNT) into FRPCs from an aqueous medium. The novel SEPPS molecule enabled not only the dispersion of SWCNTs in the aqueous medium for their introduction onto carbon fiber surfaces by spray deposition, but also reactions with epoxy resin components and fiber surfaces during the FRPC fabrication. For this purpose, the prepared SWCNT dispersions in the presence of SEPPS were introduced into the polymer-fiber interface by spray deposition onto the glass fiber fabric surfaces, which were characterized using scanning electron microscopy (SEM). Next, FRPC samples were manufactured by the vacuum infusion process from these glass fibers, and the effect of the presence of SEPPS and the content of SWCNTs at the polymer-fiber interface was investigated on the key mechanical properties resulting composite materials.

## ÖZET

### ÇOK FONKSİYONLU KARBON NANO MALZEMELERİN HAZIRLANMASI VE ELYAF TAKVİYELİ POLİMERİK KOMPOZİTLERE KATILMASI

NECDET ÖZÇELİK

Malzeme Bilimi ve Nano Mühendisliği, Yüksek Lisans Tezi, Temmuz 2021

Tez Danışmanı: Assist. Prof. Serkan Ünal

Keywords: Karbon Nanotüp, Cam Elyaf Takviyeli Polimerik Kompozitler, Vakum İnfüzyon,  
Fiber Reçine Ara Yüzü, Ultrasonik Sprey Yöntemi

Elyaf takviyeli polimerik kompozit (FRPC) malzemelerin bileşenlerinden biri olarak nanomalzemelerin kullanımının mekanik, termal ve elektriksel özelliklerini önemli ölçüde iyileştirebileceği iyi bilinmektedir. Bu tür nano ölçekli takviyelerin türü ve bunların FRPC'lere dahil edilme süreçlerinin, yüksek performanslı malzemelerin kullanıldığı havacılık, havacılık, askeri ve otomotiv gibi çeşitli sektörlerde uygulamalarını sağlamak için hem uygun maliyetli hem de endüstriyel olarak uygulanabilir olması gerekmektedir. Bir FRPC yapısındaki en hassas bölgelerden biri olan polimer matris ve fiber arasındaki arayüze nanomalzemelerin etkin bir şekilde dahil edilmesi ve düzgün bir şekilde dağıtılması, matristen fibere daha verimli bir yük aktarımı sağlayabilir. Bununla birlikte, sistematik olarak önemli iyileştirmeler elde etmek için, istenmeyen aglomerasyon, dağılma zorlukları ve yüzeyde fonksiyonelite sağlayamama gibi karbon nanomalzemelerle ilgili temel sorunların uygun şekilde ele alınması gerekir. Bu çalışmada, sulu bir ortamdan tek duvarlı karbon nanotüplerin (SWCNT) FRPC'lere dahil

edilmesi için yeni ve çok fonksiyoneliteli bir silan birleştirme ajanı (SEPPS) tasarlanmış ve sentezlenmiştir. Yeni SEPPS molekülü, yalnızca SWCNT'lerin spreyleme yoluyla fiber yüzeylere uygulanmaları için sulu bir ortamda dağılmasını değil, aynı zamanda FRPC üretimi sırasında epoksi reçine bileşenleri ve fiber yüzeyleri ile reaksiyonlarını da mümkün kıldı. Bu amaçla, SEPPS varlığında hazırlanan SWCNT dispersiyonları, cam elyaf kumaş yüzeyleri üzerine spreyleme yoluyla polimer-elyaf ara yüzüne dahil edildi ve taramalı elektron mikroskobu (SEM) kullanılarak karakterize edildi. Daha sonra, bu cam elyaflardan vakum infüzyon işlemi ile FRPC numuneleri üretildi ve SEPPS'nin varlığının ve SWCNT'lerin polimer-elyaf arayüzündeki içeriğinin, kompozit malzemelerden elde edilen temel mekanik özellikler üzerindeki etkisi araştırıldı.

*To my family*

## Acknowledgements

I would like to begin by expressing my truthful appreciation and gratitude to my supervisor, Asst. Prof. Serkan Ünal, for his immense patience, support, and encouragement throughout my M.Sc. studies. His attitude to challenges in all aspects of life, his ability to offer new views and solve problems, will always be an inspiration to me.

Also, I would like to express my appreciation to my jury members, Prof. Dr. Mehmet Yıldız and Assoc. Prof. Engin Burgaz, for dedicating their time and effort to providing constructive encouragement and advice for this thesis.

My deepest appreciations go to Ayşe Durmuş Sayar for being with me in all difficulties, Dr. Selda Erkoç İlter for always enlightening me with her knowledge and Murat Tansan for helping me during my laboratory work anytime I needed. I was very lucky to have them at my side, supporting and assisting me throughout this study. This study would not be possible without their assistance and experience. I also want to express my sincere thanks to Dr. Emine Billur Seviniş Özbulut, who had a significant role in my membership in this exclusive group. Also, I am happy to thank Deniz Anıl for her efforts to prepare this thesis. Additionally, I would like to thank the former and current fellow members of the Dr. Unal's Research Group, Buket Alkan Taş, Erdiñ Taş, Ekin Berksun, Tuğçe Çinko and Doğacan Kızılkoca.

My colleagues and friends at Sabancı University Integrated Manufacturing Research and Application Center, Dilay Serttan, Ömer Ayla, Soner Kızıl and mechanical testing and materials characterization laboratory members also deserve special thanks. I am grateful for the help I received from them throughout this study.

I cannot just thank my parents, Güven and Pınar Özçelik, my lovely sister Nevra Özçelik for her life-long existence in all my life, my grandparents Köksal and Neval Helvacı, my uncle Başar Helvacı and my aunt Bahar Helvacı Yalaz who always supported and trusted me in any condition. I am grateful to Zeliha Ece Erdoğan, who deserves much more than thanks for never leaving her love, companionship, and support for even a minute.

Finally, I am happy to thank my very close friends Berkcan Altınmakas, Aliye Ecem Kabayuka, Atahan Koyuncu, Oğuz Polat, Berkay Çiçek, Buse Önder and Umut Sayar who inspire me and make my life happier, interesting, and enjoyable with them by always being by my side.

## List Of Figures

Figure 1 SEM images of fractured surfaces of unidirectional carbon fiber reinforced polymeric composites: (A) commercial-sized carbon fiber–reinforced epoxy composite, (B) 5 wt% graphene oxide coated carbon fiber reinforced epoxy composites, (C) 10 wt % graphene oxide coated carbon fiber reinforced epoxy composite [17].....	6
Figure 2 Carbon allotropes: graphene to fullerene, nanotubes, and graphite [11] .....	8
Figure 3 (a) Schematic honeycomb structure of a graphene sheet. Single-walled carbon nanotubes can be formed by folding the sheet along lattice vectors. The two basis vectors $a_1$ and $a_2$ are shown. Folding of the (8,8), (8,0), and (10, -2) vectors leads to armchair [31] .....	10
Figure 4 Drop diameter of air-brush and ultrasonic spraying techniques [54].....	15
Figure 5 Schematic of Ultrasonic Spray Deposition [55].....	16
Figure 6 CNT Functionalization Methods.....	17
Figure 7 Typical Defects in a SWCNT [57].....	18
Figure 8 Scheme of procedure by the oxidation of CNTs by acid and oxidative gas [59].....	19
Figure 9 TEM images: (a) SWCNTs rope; (b) acid treated SWCNTs rope [61] .....	20
Figure 10 Schematic representation of CNT fluorination and subsequent alkylation [59] .....	21
Figure 11 Schematic representation of nucleophilic addition of dipyrindyl imidazolidene to CNTs [59] .....	22
Figure 12 Schematic representation of the electrophilic addition of $\text{CHCl}_3$ to CNT and hydrolysis of the functionalized CNTs [59] .....	22
Figure 13 Schematic representation of [2 + 1] cycloaddition of nitrenes and the dichlorocarbene addition [59] .....	23
Figure 14 Schematic representation of the radical addition of diazonium salts to CNTs [59].....	23
Figure 15 Schematic representation of the thiolation of CNTs [59] .....	24
Figure 16 a) Silanized CNT b) Pristine CNT [87].....	27

Figure 17 Suspension stability of the MWCNTs (A: Pristine, B: Pretreated, C: UV/O <sub>3</sub> -treated, D: Reduced, E: Silanized) [87].....	27
Figure 18 General formula of silane coupling agents.....	28
Figure 19 Reaction mechanism of trialkoxy organosilane compounds to the carbon nanotube surface.....	28
Figure 20 Coating mechanism of alkoxy silane compounds with sol-gel method.....	29
Figure 21 Ozone Oxidation Setup.....	30
Figure 22 Reaction of SEPPS with oxidized CNT.....	31
Figure 23 Schematic of SEPPS synthesis.....	31
Figure 24 Ultrasonic spray deposition of SEPPS-SWCNT aqueous dispersion on glass fiber fabric.....	33
Figure 25 TGA results of oxidized SWCNTs.....	34
Figure 26 TGA results of chemically modified SEPPS-SWCNTs.....	35
Figure 27 XPS results of pristine, and ozone treated SWCNTs.....	36
Figure 28 SWCNTs in water a) after reaction with SEPPS b) after physical mixing with SEPPS.....	37
Figure 29 Particle Size Measurements of pristine, oxidized and SEPPS-SWCNTs physically mixed.....	38
Figure 30 SEM images of a) SEPPS-SWCNT b) oxidized-SWCNTs sprayed onto glass fiber fabric by ultrasonic spray deposition.....	39
Figure 31 Demonstration of SWCNTs in water a) after reaction or b) after physical mixing with SEPPS.....	40
Figure 32 Steps of vacuum infusion process.....	43
Figure 33 Produced composite plate after vacuum infusion process.....	43
Figure 34 Tensile test specimens of CNT reinforced GF composite ( <i>left</i> ), neat GF composite ( <i>right</i> ).....	44
Figure 35 Tensile test setup.....	45
Figure 36 Tensile test specimen before ( <i>left</i> ) and after ( <i>right</i> ) tensile test.....	45
Figure 37 Tensile test results of Ox-SWCNT reinforced ( <i>top left</i> ), SEPPS reinforced ( <i>top right</i> ), SEPPS-SWCNT (2:1) reinforced ( <i>bottom left</i> ) and, SEPPS-SWCNT (1:1) reinforced ( <i>bottom right</i> ) FRPC samples.....	48

Figure 38 Tensile test results of FRPC samples containing 10 mg/m <sup>2</sup> (top left) 20mg/m <sup>2</sup> (top right) and, 30 mg/m <sup>2</sup> (bottom) carbon nanomaterials in comparison with reference and only SEPPS containing samples.....	48
Figure 39 Changes in the Young's Modulus values of FRPC samples containing Ox-SWCNTs, SEPPS or SEPPS-SWCNT mixtures in comparison with the reference.....	49
Figure 40 Changes in the tensile strength values of FRPC samples containing Ox-SWCNTs, SEPPS or SEPPS-SWCNT mixtures in comparison with the reference.....	50
Figure 41 Storage modulus of reference and selected nano-reinforced FRPC samples.....	51
Figure 42 Tan delta results of reference and selected nano-reinforced FRPC samples .....	51
Figure 43 DSC thermograms of reference and selected nano-reinforced FRPC samples.....	52

## Table of Contents

<b>CHAPTER 1 .....</b>	<b>1</b>
<b>1. INTRODUCTION.....</b>	<b>1</b>
1.1. Motivation .....	1
1.2. Objectives .....	2
1.3. Outline .....	3
<b>CHAPTER 2 .....</b>	<b>4</b>
<b>2. LITERATURE REVIEW .....</b>	<b>4</b>
2.1. Graphene and Graphene Oxide (GO) .....	7
2.2. Carbon Nanotubes (CNTs) .....	8
2.2.1. Structure .....	8
2.2.2. Properties of CNTs .....	10
2.2.3. Applications of CNTs.....	12
2.2.4. Processing of CNTs.....	12
2.3. Ultrasonic spray deposition .....	14
2.4. Chemical functionalization of CNTs.....	16
2.4.1. Covalent functionalization of CNTs.....	17
2.4.2. Non-covalent surface modifications of CNTs .....	24
2.5. Silane coupling agents.....	25
2.5.1. Coupling mechanisms of silane compounds .....	27
<b>CHAPTER 3 .....</b>	<b>30</b>
<b>3. FUNCTIONALIZATION, DISPERSION AND ULTRASONIC SPRAY DEPOSITION OF CNTs.....</b>	<b>30</b>
3.1. Materials .....	30
3.2. Ozonolysis of CNTs .....	30
3.3. Design of a novel, multi-functional silane coupling agent .....	30

3.3.1.	Synthesis of 3-((2-aminoethyl) (3-(trimethoxy silyl) propyl) ammonium) propane -1-sulfonate (SEPPS) .....	31
3.4.	Preparation of SEPPS incorporated SWCNTs .....	32
3.4.1.	Preparation by chemical reaction .....	32
3.4.2.	Preparation by physical mixing .....	32
3.5.	Dispersion of SEPPS incorporated SWCNTs .....	32
3.6.	Ultrasonic spray deposition of SWCNTs .....	32
3.7.	Results and Discussion .....	33
3.7.1.	Thermogravimetric analysis of oxidized SWCNTs.....	33
3.7.2.	X-Ray Photo-Electron Spectroscopic (XPS) analysis .....	35
3.7.3.	Dispersion of SEPPS-SWCNTs .....	36
3.7.4.	Scanning Electron Microscope (SEM) analysis .....	38
3.8.	Conclusions .....	39
<b>CHAPTER 4 .....</b>		<b>41</b>
<b>4.</b>	<b>PRODUCTION and CHARACTERIZATION of FRPCs CONTAINING CNTs .....</b>	<b>41</b>
4.1.	Materials .....	41
4.2.	Preparation of aqueous SWCNT dispersions .....	41
4.3.	Spray deposition of aqueous SWCNT and SEPPS/SWCNT dispersions onto glass fiber fabrics	41
4.4.	Composite production by Vacuum Infusion Method .....	42
4.5.	Sample preparation for mechanical, thermal and structural characterizations .....	44
4.6.	Results and Discussion .....	45
4.6.1.	Structural characterization of FRPCs .....	45
4.6.2.	Mechanical characterization of FRPCs .....	46
4.6.3.	Thermo-mechanical Analysis of FRPCs .....	50
4.6.4.	Thermal Characterization of FRPCs.....	51

<b>4.7.</b>	Conclusions .....	52
-------------	-------------------	----

# CHAPTER 1

## 1. INTRODUCTION

### 1.1. Motivation

Due to their superior mechanical, thermal, structural, and corrosion resistance combined with their low density, fiber reinforced polymeric composite materials (FRPC) are high performance, load bearing structures. They have been garnering considerable interest in a variety of industries, including aerospace, transportation, marine, and wind energy [1]. FRPCs have been utilized as structural engineering materials and are usually composed of a polymer matrix and reinforcing elements such as carbon or glass microfibers, as well as metallic or organic fillers[2]. Recently, industrial requirements, particularly in the aircraft industry, have evolved towards significantly stronger, durable, and lighter-weight polymeric composites; as a result, mechanical properties of composite structures reinforced in the microscale are needed to be further enhanced, possibly through the incorporation of nanoscale reinforcement agents. While the main reinforcements are microscale glass or carbon fiber fillers in FRPCs, secondary reinforcements might be used in the form of carbon nanostructures such as carbon nanotubes (CNTs) or graphene. It is important to note that as high as 30 to 60% of fiber reinforcing materials are used in traditional microscale composites, whereas only a small content of the nano-scale reinforcement may be required to achieve significant improvements in mechanical, thermal, and electrical properties, resulting in the development of multifunctional composite materials [2]. In terms of their industrial feasibility, FRPCs reinforced with nanostructures are expected to be financially sustainable and readily producible by existing or new manufacturing techniques.

With these considerations in mind, our study has focused on the incorporation of carbon nanomaterials into FRPCs in a manner that can be scaled up to commercial applications and provide a fresh viewpoint on the structure-property-process relationships in these materials. Numerous methods have been reported for the incorporating nanostructures into neat polymers or polymeric composites in the literature. The most noteworthy examples include the incorporation of nanomaterials via resin infusion, growth on carbon fiber surfaces by CVD, electrophoretic deposition, and interlayer placement. However, critical issues might arise in the aforementioned approaches during the incorporation of nanomaterials into FRPCs in large scales. These inevitable fundamental problems of the research, such as dispersion, alignment,

and compatibility with the polymer matrix, remain unresolved. In this study, ultrasonic spray deposition was selected as a comprehensive technique for the individual and uniform incorporation of carbon nanomaterials in the presence of a chemically functional dispersing agent into FRPCs produced by the vacuum infusion method.

Since Ajayan's first research in 1994 [3], the fabrication of CNT reinforced polymeric composites quickly became one of the most exciting research topics. Although extensive research studies have been published comprising CNTs, relatively only a few higher TRL examples and businesses exist on the successful industrial applications of CNTs. Additionally, chemically modified CNTs have been extensively studied to substantially enhance the mechanical characteristics of nanocomposites by creating reactive sites with the polymer matrix [4]. This is referred to as chemical functionalization. Additionally, the interfacial properties of FRPCs improved with nanomaterials have been addressed between the nanotube and the polymer matrix, nanotube and reinforcing fibers, and polymer matrix and reinforcing fibers, to enable an effective load transfer through these interfaces. Thus, it is hypothesized that the functionalization of CNTs placed at the polymer matrix-fiber interface might flawlessly improve the interfacial characteristics of FRPCs [5]. Additionally, the dispersion quality of CNTs might be improved by chemically altering the nanotube surface structure or the dispersion formulation to create strong interactions with the dispersion medium [6].

## **1.2. Objectives**

This thesis introduces the synthesis and characterisation of a novel silane compound (SEPPS) capable of forming a strong chemical bond with the polymer matrix, reinforcement fibers and CNT surfaces while also improving the dispersibility of CNTs in the aqueous medium. Thus, a detailed investigation of the effect of the nano-reinforcement at the interface, introduced by the ultrasonic spray deposition of CNTs in the presence of SEPPS onto fiber surfaces, on the mechanical properties of FRPCs was carried out. The newly developed, novel silane coupling agent, SEPPS, enabled the preparation of multi-functional nanomaterial dispersions that can readily be used in large scale productions of FRPCs and their commercial applications. For this purpose, ultrasonic spraying technique was utilized to introduce CNTs in the presence of SEPPS multi-functional materials from an aqueous medium onto fabric surfaces followed by vacuum infusion process for the production of FRPC panels.

### **1.3. Outline**

Chapter 2 provides background information and provides an in-depth examination of the use of carbon nanomaterials, specifically carbon nanotubes and graphene in FRPCs with a discussion of the state of the art functionalization and incorporation methods, along with the challenges encountered in these applications. Additionally, the method of ultrasonic spraying, the chemistry of silane coupling agents, and their applications with nanomaterials were thoroughly reviewed. The third chapter presents the experimental methodology and characterization results for the newly synthesized, multi-functional silane coupling agent, SEPPS, dispersion of carbon nanomaterials in water in the presence of SEPPS, and their placement on fiber surfaces via ultrasonic spray deposition method. The fourth chapter presents the experimental methodology and characterization results for the production of FRPC panels by vacuum infusion, and the investigation of the mechanical properties of resulting composite structures containing carbon nanomaterials at the polymer-fiber interface.

## CHAPTER 2

### 2. LITERATURE REVIEW

Thanks to the rapid advances in the defence, aerospace and aviation industries, the need for structural materials with low weight and high strength is increasing day by day [3]. With their excellent structural and transport properties such as high strength, modulus, electrical conductivity, flexibility, and thermal stability [7], carbon nanomaterials are often preferred in the production of sensors, water treatment media, biomedical and composite materials. Examples of nanomaterials belonging to the carbon family mostly used in the reinforcement of composite materials are single and multi-walled CNTs (MWCNT), graphene, and fullerene.

After the discovery by Sumio Iijima in 1991, the use of CNTs in various polymeric nanocomposites has increased dramatically over time. CNT-polymer interactions can improve the strength and toughness of materials which are especially desired in automotive, aerospace and leisure applications. CNTs have been incorporated into various other commercial products such as rechargeable batteries, water filters, thin film electronics, actuators, and lightweight electromagnetic shields as well [8].

Recent examples of FRPCs containing CNTs include fuselage of aircrafts, propellers of helicopters, chassis of automobiles and wind turbine blades. In principal, if these materials are to be benefited as effective reinforcements in FRPCs, excellent dispersion, and interfacial bonding between CNTs and polymer matrix must be provided[7]. It has been previously reported that the incorporation of 1 wt% MWCNTs into the epoxy resin matrix, can increase the stiffness and toughness up to 6% and 23%, respectively without negatively affecting any other mechanical properties[8]. However, due to the intrinsic nature of CNTs and their agglomeration caused by Van der Waals forces, their homogeneous dispersions cannot be easily achieved in water, organic solvents, or polymers [9]. Ultrasonication, calendaring, ball milling or chemical modification methods can be used to enable a homogeneous distribution of carbon nanomaterials. These methods can be used alone or as complementary to each other. Although the ultrasonication, calendaring, and ball milling methods, which can be classified as physical methods, are frequently used, they might not be effective when used alone due to reasons such as re-agglomeration after the process as a function of time[10]. The surface modification of carbon nanomaterials for homogeneous dispersion of flocculated carbon nano-additives has attracted considerable attention in recent years. Stable and homogeneous distributions of them can be achieved by creating active sites on the surfaces of carbon nanomaterials by

functionalizing them with groups that are compatible with the desired liquid medium or polymer matrix (i.e., epoxy resin).

Over the last decade, graphene and graphene oxide have also generated enormous attention owing to their unique and superior electrical, optical, mechanical, and chemical characteristics.[11]

At sufficiently high loadings, the entanglement of long CNTs in a matrix may result in unacceptably significant viscosity increases, while graphene platelets can more readily slide past one another, thus reducing the viscosity increment. Thus, from a processing perspective, thermoset resins treated with graphene may be preferred over CNTs for advanced FRPCs [12]. The functionalization of graphene to increase its compatibility with the monomer or precursor of resins may further aid in controlling the solution viscosity. During the curing process, an external field, usually an electrical field, may also be employed to orient or align graphene in thermosetting polymers [13].

Lee et al. [14] used a technique devised by a Princeton University research group [15], [16] to produce thermally exfoliated graphene oxide. The functionalized graphene single sheet formed as a consequence, included C-OH and -COOH groups. Such functionalized graphene was used to modify epoxy resins, resulting in an increase in strength and toughness of by approximately 30% and 200-700% at room and low temperatures of -130 °C, respectively, with a decrease in thermal expansion coefficient at both below and above  $T_g$  of approximately by 25% at 1.6 wt% functionalized graphene loading, and an increase in  $T_g$  by approximately 8°C at 0.4 wt% loading, all without deteriorating the processability. The modified epoxy resin showed potential for utilization in next generation FRPC-based multifunctional cryo-tank applications.

Additionally, graphene nanoparticles may be doped into the surface of fiber reinforcement, creating a three-dimensional effect between plies when loaded. This approach is expected to show a notable impact on the fiber-matrix interface, altering the interlaminar fracture toughness, hardness, and delamination resistance, among other properties. Literature studies also describe the use of graphene doped fibers for strain monitoring, pressure sensing, and fluid flow monitoring applications [12].

Numerous coating techniques, including soaking, dip coating, electrospraying, and electrophoretic deposition, have been employed to coat continuous fibers, fiber textiles, or woven fibers with nanomaterials, which may be utilized as-is or cut down to short fibers for use in processes such as sheet moulding compound or melt compounding.

Graphene oxides may be dispersed in fiber sizing chemicals and then coated on the surface of fibers by pulling or dipping the fibers through the modified sizing agent. The interfacial shear strength (IFSS, which measures the microbond of a single fiber to matrix) of epoxy composites containing coated carbon fiber was increased by up to 70.9 %, while the interlaminar shear strength (ILSS, which measures the interlaminar bonding of composites) was increased by 12.7 % compared to the composite containing de-sized and commercially sized carbon fiber, respectively [17]. Additionally, the tensile strength and modulus of graphene oxide coated carbon fiber reinforced epoxy composites were much greater than those of uncoated carbon fiber reinforced epoxy composites. The microscopic examination (Figure 1) revealed that the commercial-scale carbon fiber composites failed mostly due to gradual interfacial debonding and fiber pullout, followed by fiber breaking. The surface of the extracted fibres was clean, suggesting a poor interfacial connection between matrix and fiber. In comparison, graphene oxide coated carbon fiber composites demonstrated simultaneous fiber and matrix failure, whereas the interfaces between the fiber and matrix remained almost intact even after failure, indicating strong interfacial bonding.

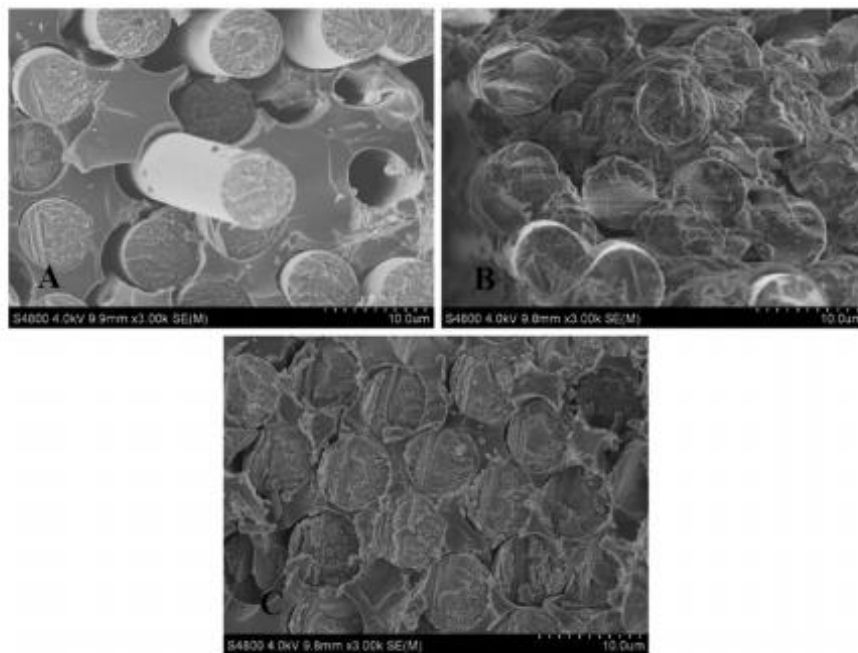


Figure 1 SEM images of fractured surfaces of unidirectional carbon fiber reinforced polymeric composites: (A) commercial-sized carbon fiber–reinforced epoxy composite, (B) 5 wt% graphene oxide coated carbon fiber reinforced epoxy composites, (C) 10 wt % graphene oxide coated carbon fiber reinforced epoxy composite [17]

## 2.1. Graphene and Graphene Oxide (GO)

Graphene is a carbon-based nanomaterial with a single carbon atom-thick, sheet structure [18], whereas fullerene is a cage structure as synthesized by Robert Curl et al. [19] in 1985. It was four years later in 1989, Krätschmer [20] verified the cage structure of C<sub>60</sub>-fullerene. In 2004, Novoselov et al. [21] used a microcomputer peeling technique to effectively remove graphene from its monolithic form, challenging the scientific understanding of two-dimensional crystals. Graphene's structure is shown in Figure 2, which is comprised of an independent layer of sp<sup>2</sup> hybrid carbon atoms. It is a two-dimensional carbon-based material with a hexagonal honeycomb crystal structure and a hexagonal honeycomb crystal structure. With a sheet thickness of 0.34 nm, graphene is the thinnest and strongest nanomaterial known so far [11]. Each carbon atom in graphene is connected through a bond to three neighbouring carbon atoms. Due to their inability to make bonds, the remaining p electrons most likely form a bond with the surrounding atoms, and the bonding orientation is perpendicular to the graphene plane. Graphene's structure is very stable, with a C–C bond length of just 0.142 nm [22]. Graphene has an extremely strong bond between each carbon atom. When an external force is applied to graphene, the atomic surface deforms and bends further to compensate for the external force. As a result, no rearrangement or misalignment of the carbon atoms occur, resulting in a continuously stable structure [23]. When graphene electrons travel in their intrinsic orbits, there is no scattering caused by external atoms or lattice imperfections [24], [25]. Graphene's exceptional characteristics are due to its unique lattice structure. There are many ways for producing graphene nowadays, but the most common ones include mechanical stripping, liquid phase stripping, chemical vapor deposition, epitaxial growth, and redox approaches [26]. Recent research has focused on graphene quantum dots, as well as carbon doped with other elements, chemicals, and organic compounds [11]. In comparison to graphene (G), graphene oxide (GO) has the benefits of being inexpensive to produce, scalable, and simple to process. It is often utilized as a precursor in the reduction of graphene oxide (RGO) [27]. Recent research studies on GO have shown that GO also has outstanding characteristics, including a high concentration of active oxygen-containing functional groups [28]. These oxygen-containing groups or decreased doping elements may be utilized as catalytic active centers for covalent/non-covalent interaction-based design, depending on the application requirements. Additionally, the presence of oxygen-containing groups broadens the GO interlayer gap. Small molecules or polymer intercalations may be used to functionalize it. A significant progress has been made in the functionalization graphene oxide and its use has been demonstrated in

desalination, medication delivery, oil–water separation, immobilized catalysis solar cells, energy storage, healthcare, and other areas [11].

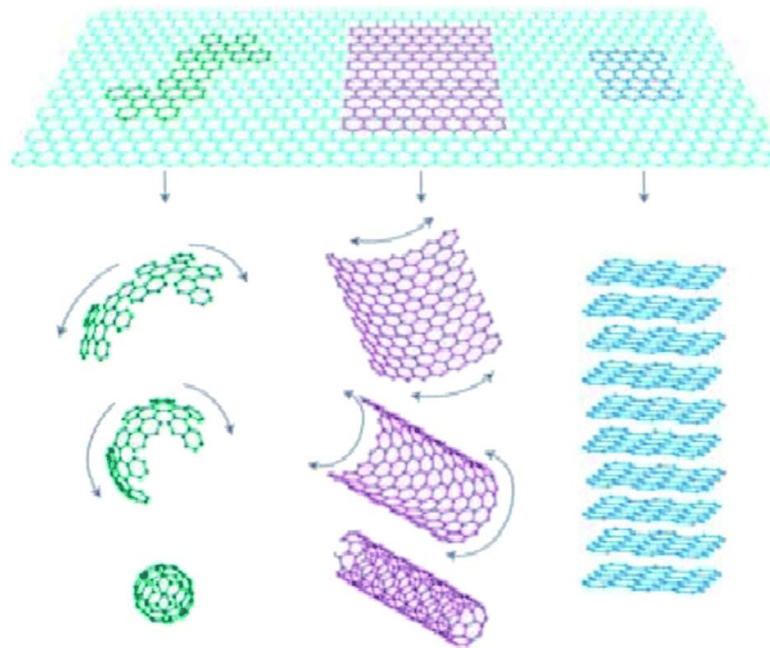


Figure 2 Carbon allotropes: graphene to fullerene, nanotubes, and graphite [11]

## 2.2. Carbon Nanotubes (CNTs)

### 2.2.1. Structure

Properties such as high mechanical strength, high conductivity, chemical inertness, stiffness, high aspect ratio and unique atomic structure have led scientists to incorporate CNTs into conventional engineering materials. CNTs are cylindrical carbon-based structures which are composed of rolled up single layer carbon sheets (graphene). The length of CNTs is in the order of micrometres. They can be single walled (SWCNT) with a diameter of less than 1 nm or multi-walled (MWCNT) with diameters reaching up to 100 nm by more than one CNTs are interlinked concentrically [29].

CNTs are comprised of folded graphitic sheets that are rolled into a concentric, cylindrical, and hexagonal lattice structure. Graphite and diamond are two allotropes of the carbon atom as solid phases. Isotropic strong diamond is obtained by sharing four valence electrons equally in carbon atoms. Graphite is created by sharing three of these valence electrons with neighbouring atoms over a covalent structure in a plane, while the fourth electron is inclined to be shared between all atoms. The type of  $sp^2$  bond produces weak van der Waals bonding forces from the planar graphite sheet while creating strong internal forces in the plane sheets. The form of  $sp^2$  bonding induces high intrinsic forces in plane graphitic sheets but weak van der Waals bonding forces.

Nanotubes also have a carbon backbone that is  $sp^2$  bonded. Graphitic layers may form concentric structures because of definite topological defects in nanotubes. Disorders in bulk CNTs generate pentagons, heptagons, and other defects within the sidewalls that normally disrupt desired unique properties of CNTs, while all carbons in well-organized CNTs are bonded in a hexagonal lattice except at their ends [8]. Nanotubes are classified into two categories based on the number of inner graphene layers and whether they have open or closed ends. The multi-walled carbon nanotubes (MWCNT) are one type of them. It was first found as the form of concentric cylinders arranged along a common axis, identical to hollow graphite fibers. The composition of MWCNTs is much more regular than that of graphite fibers. The distance between each graphite layer and the MWCNTs is 0.34 nm, marginally more than the single crystal value of 0.335 nm. Because of various geometrical limitations in shaping concentric cylinders without wrinkles when maintaining and preserving the space between each graphite layer, this smaller distance was obtained [30]. The hexagonal honeycomb graphene structure is formed into a cylindrical shape with  $(m,n)$  lattice vector boundary conditions, resulting in a single-walled carbon nanotube (SWCNT) (Figure 3). This graphene structure schematic characterizes the essential properties of each nanotube, and each nanotube has the main symmetrical structure [31]. This second kind of CNT has a uniform diameter of 1- 2 nm, while MWCNTs have a diameter of 5 to 20 nm. MWCNT diameters can even reach 100 nanometers [8]. The lattice vector indices  $(m, n)$  are used to specify them, and the nanotubes are often categorized according to their folding characteristics. When  $n=0$ ,  $(m,0)$ , CNTs are pointed to as “zigzag,” and when  $m=n$   $(m,m)$ , CNTs are pointed to as “armchair.” In certain cases, they are referred to as "chiral". In Figure 3, the unit vectors of the hexagonal lattice are paired with a graphene layer. Metallic properties such as whether each CNT wall is metallic or semiconducting are determined by the chiral angle between the tube axis and hexagons [31]. Specific SWCNT may show thermal conductivities greater than the thermal conductivity of diamond [8].

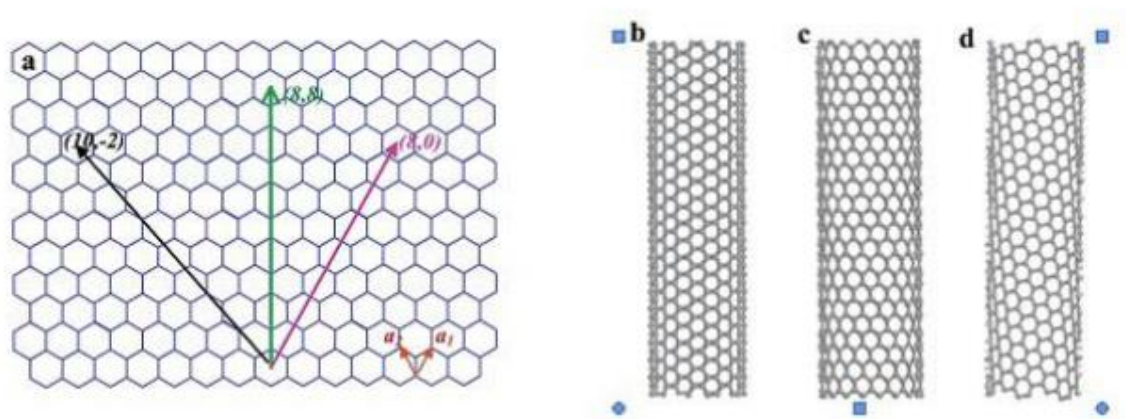


Figure 3 (a) Schematic honeycomb structure of a graphene sheet. Single-walled carbon nanotubes can be formed by folding the sheet along lattice vectors. The two basis vectors  $a_1$  and  $a_2$  are shown. Folding of the (8,8), (8,0), and (10, -2) vectors leads to armchair [31]

## 2.2.2. Properties of CNTs

Nanotubes are unique because of their unique combination of dimension, form, and topology, which results in a wide variety of superior properties. The C-C bond network in the structure provides a huge strength and stiffness to the material and ascribe CNTs as one the most promising components for high-performance materials such as structural composites. Furthermore, nanomaterials offer a wide surface area, which can be useful in mechanical and chemical applications. BET methods are typically employed to determine the surface area of MWCNTs, which is reported as 10-20 m<sup>2</sup>/g, greater than graphite but lower than activated porous carbons. SWCNTs are supposed to have surface areas that are an order of magnitude greater.[30]

### 2.2.2.1. Mechanical properties of CNTs

Mechanical properties such as elastic modulus, stiffness and strength are the most important parameters in high-performance material applications. CNTs' exceptional properties were proven by theoretical and experimental studies. Wong et al. reported the first direct calculation in 1997. The stiffness constant of arc-MWCNTs pinned at one end was measured using an atomic force microscope (AFM). This resulted in an average Young's modulus of 1.28 TPa. More specifically, they were able to take the first strength measurements, achieving a bending strength of 14 GPa on average [32]. However, experimental studies are challenging because of the extremely small size of CNTs. Therefore, results of different studies show significant

variability. Differences in structure, synthesis technique or various defects can cause different results as well. For example, Lourie and Wagner reported Young's moduli of 2.8-3.6 TPa for SWCNT and 1.7-2.4 TPa for MWCNT [33]. On the other hand, Yu et al. claims that Young's moduli of SWCNT's differs from 320 GPa to 1470 GPa, and MWCNT's from 270 GPa to 950 GPa [34]. Salvetat et al. used the AFM to obtain Young's modulus values of 12 to 50 GPa during bending and manipulation in the first calculations for CVD growth MWCNT [35].

#### **2.2.2.2. Thermal and electrical properties**

According to well established studies [36], the electron transport parameters of tubes are well characterized around the outer layer. McEuen and colleagues deposited SWCNTs on a surface area using AFM and then utilized metal electrodes to connect the nanotubes [37]. Therefore, surface modification of CNTs drastically altered their electrical properties. The remarkable conductivity characteristics of nanotubes have been investigated in recent years by the electron transport system, termed 'ballistic,' discovered in each MWCNT at room temperature [30], [35], where they act as metals or very tiny band gap semi-conductors, depending on the chiral angle [30], [35]. SWCNTs' electronic characteristics have been studied more widely rather than MWCNTs since measurements of the electron transport process on each SWCNT are considerably more visible [30]. The band gaps of semiconducting nanotubes are inversely proportional to their diameters. It is around 1.8 eV for small diameter nanotubes and 0.18 eV for the highest diameter, stable SWCNT. Because of their one-dimensional structure, pure nanotubes have an extraordinarily high conductivity and a very low resistance. This enables it to conduct the charge through the nanotubes without dispersing; as a result, heat build-up is minimized. Nanotubes can conduct current at extraordinarily high densities of up to 100 MA/cm<sup>2</sup> [38].

Thermal conductivity of nanotubes is also rather high at room temperature, reaching up to 6000 W/mK; however, value as low as about 200 W/mK, or as high as 3000 W/mK has been reported for MWCNTs [35].

#### **2.2.2.3. Chemical inertness**

CNTs are comprising of non-reactive graphite lattice structure. Therefore, they are inert and C-C bonds among the structure of nanotubes do not lead to reactions with other functional groups. The only way to react CNTs with other chemical groups is to disrupt its chemical structure to create functional groups on the sidewalls or tube ends [30].

### **2.2.3. Applications of CNTs**

MWCNTs were first used as electrically conductive fillers in plastics, with amounts as low as 0.01 wt% forming a percolation network due to their high aspect ratio. At 10 wt% loading, disordered MWCNT-polymer composites have conductivities as high as  $10,000 \text{ Sm}^{-1}$ . Conductive CNT containing plastics have allowed electrostatic-assisted painting of mirror housings, as well as fuel lines and filters that dissipate electrostatic charge in the automotive industry. Electro-magnetic interference (EMI)-shielding kits and wafer carriers for the microelectronics industry are among other applications. CNT powders mixed with polymers or precursor resins can improve the stiffness, strength, and hardness in load-bearing applications. Adding 1 wt% MWCNT into epoxy resin increases stiffness and crack resilience by 6% and 23%, respectively, without sacrificing other mechanical properties [8]. Zhiwei et al. studied mechanical performance of carbon fiber reinforced polymeric composites modified with CNTs in the matrix and the interface and reported that the introduction of MWCNTs onto the fiber surface improves the tensile strength up to 25% [39]. The contribution of CNTs to mechanical properties pose a huge potential for use in industries such as automotive, aircraft and marine.

### **2.2.4. Processing of CNTs**

#### **2.2.4.1. Dispersion**

The dispersion of CNTs in solvents or polymeric matrices directly affects the quality and performance of composite materials reinforced with them. Since CNTs are an intrinsically inert materials which can easily agglomerate and entangle due to their size and high aspect ratio, proper dispersion, and strong interfacial bonding between the CNTs, and the polymer matrix must be ensured if these materials are to be used as efficient reinforcing materials in polymer composites [40]. In the literature, mainly two type of dispersion methods exist for a proper dispersion; mechanical and chemical methods. Bath ultrasonication, probe ultrasonication, milling, grinding and high shear mixing are considering as mechanical methods while ozone treatment, acid treatment, surface functionalization and surfactant-assisted systems as chemical methods. Numerous studies have been done to examine the interaction of CNTs among themselves and with other media in the literature [7].

#### **2.2.4.2. Incorporation of CNTs into polymeric composites**

Carbon nanotubes are introduced into polymeric composites by two different approaches. The first strategy is the addition of CNTs into polymeric resins and then impregnation of the CNT-resin mixture to the primary fibers. Unlike the first strategy, second approach is the integration

of CNTs onto the fibers and then the impregnation of neat resin to the CNT-decorated fibers [41]. There are several methods for the incorporation of CNTs either into polymeric resin or onto fiber surfaces.

#### **2.2.4.2.1. Incorporation of CNTs by resin infusion**

As resin infusion is the most scalable and practical procedure for the production of FRPCs in various industrial applications, it is also commonly utilized for the incorporation of CNTs that includes an initial dispersion procedure into the resin, followed by liquid injection molding to infuse the CNT-resin mixture into the fiber assembly for the construction of the final composite structure. On the contrary, the amount of CNTs that can be added into resin is constrained due to the dispersion, viscosity, and infiltration problems. The consistency of the dimensions of nanotubes must be ensured for excellent fabrication. Besides, the number of individual nanotubes must be in a suitable range which provides the best dispersion. Furthermore, the viscosity of the resin increases excessively due to the relatively high loading of CNTs. Because of higher viscosity, unimpregnated regions and dry spots are observed in composite structure. Specifically, nanotube concentrations more than approximately 1 vol.% aggravate the mechanical performance of the final composites, resulting in a considerable reduction in reinforcing ability [42]. As a result, this approach is regarded as the most difficult of all integration approaches.

#### **2.2.4.2.2. Growth of CNTs on carbon fiber substrates**

To enhance the interfacial characteristics of the composites, CNTs can be produced directly onto the reinforcing fiber substrates using the chemical vapor deposition (CVD) technique in the presence of a catalyst. The polymeric resin is subsequently injected into this assembly using the appropriate composite production procedure. The dispersion and alignment of nanotubes, as well as the composite characteristics, may be adjusted using this approach in the thickness direction. However, there are challenges in the CNT development process, such as the inability to develop CNTs in large surface areas, catalyst constraints, difficulties for the functionalization of nanotubes formed on the main reinforcing fiber surfaces, and microfiber degeneration due to the CVD method's extreme growing conditions [43].

CNTs incorporated at the fiber/matrix interface by CVD have been reported to increase the composites' interfacial shear strength, according to Thostenson et al. [44]. The application of catalyst to the fiber surface, on the other hand, resulted in a considerable reduction (32%) in the interfacial strength.

#### **2.2.4.2.3. Interlayer placement of CNTs**

Another approach for the incorporation of CNTs, known as "interlayer placement," has been created as direct insertion of nanotubes between the main reinforcing fiber plies before the composite manufacturing process, since the main micron-sized fiber has the potential to be harmed by the CNT development process, and the uniformity and purity of surface grown CNTs cannot be readily regulated. This approach has the benefit of vertically aligning nanotubes, which improves out-of-plane characteristics [43]. Garcia et al. [45] were the first to successfully align CNTs on a silicon substrate and transfer them in the thickness direction onto the main fiber ply. On unidirectional prepreg carbon fiber composite, this results in a 2.5-fold rise in initial Mode I value and a 3-fold rise in initial Mode II value. In contrast to its benefits, this technology has the drawback of being an unpractical procedure in the industry owing to constraints in large-scale manufacturing, cost, and thickness fluctuations in manufactured composite structures.

#### **2.2.4.2.4. Electrophoretic deposition of CNTs**

The electrophoretic deposition (EPD) approach, which is based on applying an electrical field to charged particles distributed in a liquid media, is another approach for the incorporation of CNTs into FRPCs. CNTs are often utilized as particles in solution and are charged using a bias voltage. Consequently, charged particles are able to migrate and deposit themselves on the carbon or glass fabric substrate. EPD of both untreated and functionalized CNTs on the fiber substrate has been shown to provide uniform deposition as well as being a viable, scalable, and cost-effective technique [46]. However, challenges in controlling CNT alignment and inadequate chemical interaction with carbon fibers have been identified as limitations of this EPD approach [43]. EPD of carboxylic acid functionalized MWCNTs onto the electrically insulating primary glass fiber substrate exhibited a considerable improvement in interfacial shear strength when compared to pristine glass fiber composite materials in a recent study by Zhang et al. [6]. Furthermore, contrast to CNT development, EPD of carboxylated CNTs onto carbon fiber has little effect on in-plane characteristics [47].

### **2.3. Ultrasonic spray deposition**

Spray coating is one of the most cost-effective and versatile ways for producing thin surface coatings [48]. Spray coating, unlike other coating methods, does not need a flat substrate, specialized substrate chemistries for nanomaterial chemical development, or high pressures and temperatures on the substrates [49]. Spray coating enables for excellent control of coating

thickness due to its layer-by-layer methodology. In addition, recent advancements in spray coating have enhanced the surface homogeneity [50] and mechanical characteristics of spray coated materials [51].

Spray coating has previously been utilized to make graphene [52] and carbon nanotube films with enormous surface areas. Airbrush spraying techniques and ultrasonic spray coating are the two most used spray coating procedures. Using a pressurized gas carrier, an aerosolized dispersion of particles is applied by airbrush spray coating. CNT coatings as substrates for stem cell differentiation, CNT-based solar cell counter electrodes, and graphene-based semiconductors have all been produced using airbrush spray coatings [48].

Ultrasonic spray coating is a recent technique that utilizes a high frequency operated nozzle to produce more homogeneous droplets than airbrushing, with individual droplet quantities as small as picoliters [53] (Figure 5). The comparison of drop diameter of ultrasonic spraying and traditional airbrush is shown in Figure 4.

Ultrasonic spray nozzles, unlike airbrush techniques, distribute nanomaterials homogeneously because ultrasonic vibrations destroy particle aggregates, and the nozzle self-cleans to avoid nanomaterial build up at the spray head. For the fabrication of graphene-CNT composite electrochemical cells and CNT-based photovoltaics, ultrasonic spray coating of carbon nanomaterials has been explored [54].

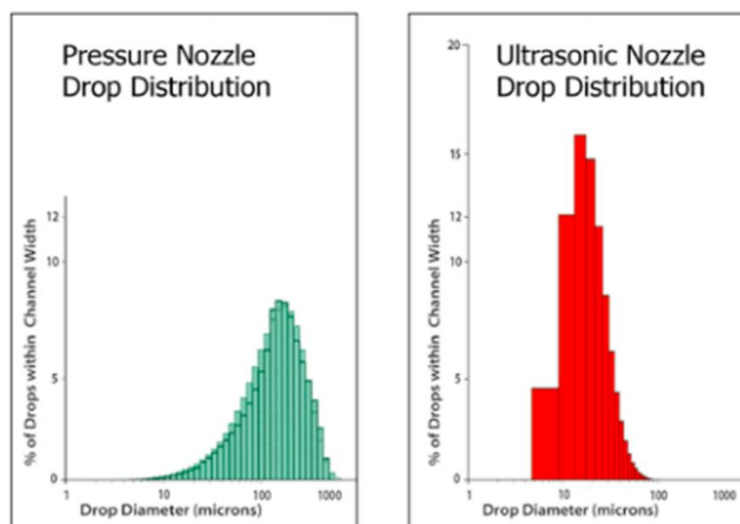


Figure 4 Drop diameter of air-brush and ultrasonic spraying techniques [54]

While ultrasonic spray coating of carbon nanomaterials has been successful in the laboratory, the absence of strong chemical (covalent) bonding between the particles is a major hurdle that must be solved before this approach (or other deposition techniques indicated above) can be used for large-scale 2D and 3D printing of all carbon nanomaterials for many practical applications. For example, graphene and CNT coatings offer a great promise for orthopaedic devices. However, owing to a lack of chemical connections between individual particles, these coatings lack structural strength, which may contribute to nanoparticle-related toxicity issues [48]. Components created utilizing carbon nanomaterials that are 2D or 3D structures must also be robust and able to tolerate different mechanical stresses for certain photovoltaic applications, such as solar panels. As a result, chemical interactions between individual nanomaterials that increase component structural stability might be useful [48].

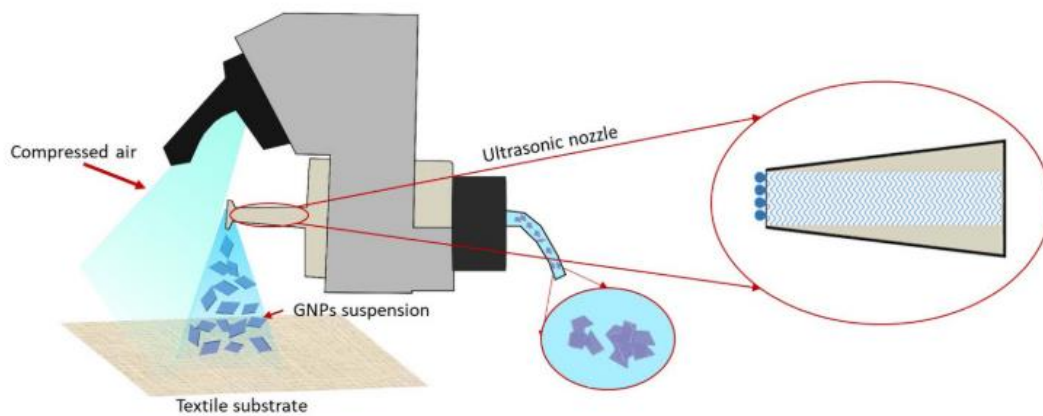


Figure 5 Schematic of Ultrasonic Spray Deposition [55]

#### 2.4. Chemical functionalization of CNTs

One of the previously stated uses of CNTs is their incorporation into FRPCs for improved characteristics. Because CNTs have a wide length-to-diameter ratio (aspect ratio) and are chemically inert, they readily form agglomerates in any organic solvent or polymer matrix, creating a great challenge during their dispersion and introduction into composite materials for possible industrial applications. By restricting the optimal load distribution through the interface, these problems immediately promote interfacial failure between the reinforcing material and the polymer matrix. Consequently, poor integration of these nanoparticles in FRPCs may cause significant mechanical property deficiencies in these materials, as well as a reduction in the durability of associated composite parts of applications, particularly in the aerospace industry.

Because of these difficulties, CNTs must be diligently treated when placed at the interface of FRPCs to guarantee a homogenous distribution of individual nanotubes, taking into account the diameter of carbon or glass fibers (typically between 6 and 12 micron). The diameter of these CNT bundles might be close to the micron sized primary fibers if they are not dispersed homogeneously and separately, allowing the formation of CNT bundles. Throughout this scenario, the bundles may behave as defects, harming the FRPCs' integrity and interfacial strength. The improvement of interfacial interactions between primary reinforcing fiber and the polymer matrix in FRPCs by the incorporation of CNTs at this interface depends on the nature and concentration of chemical functional groups attached to the surface of CNTs, which directly affects the dispersibility and wettability, as addressed in this thesis and analyzed in depth. Individually isolated CNTs are the only way to establish a durable interface in FRPCs, as previously documented in the literature [56]. Significant research efforts have been directed to the chemical modification of the surface of CNTs, which is referred to as "chemical functionalization," to overcome stated limits of CNTs, distribute them evenly, and enhance their interactions with other components of composite materials. Surface modification techniques may be subdivided into covalent and non-covalent functionalization (Figure 6), with each form of functionalization resulting in a controllable degree of contact between CNTs and the surrounding materials.

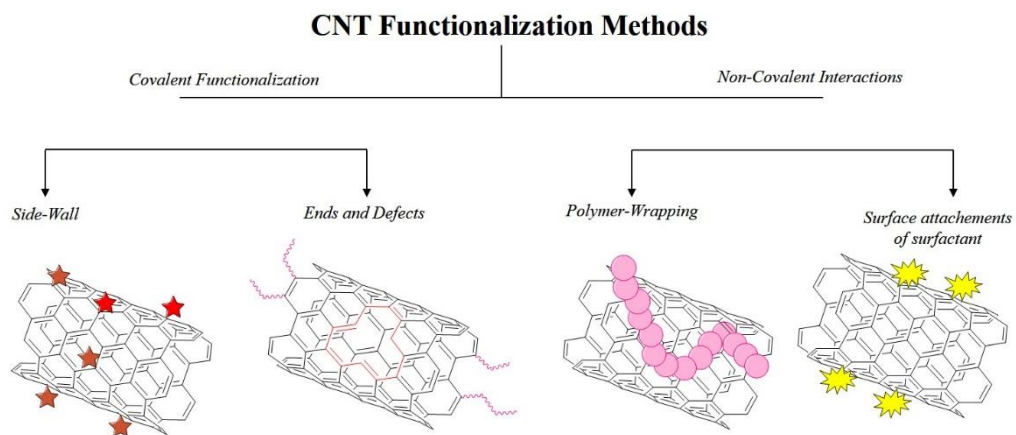


Figure 6 CNT Functionalization Methods

### 2.4.1. Covalent functionalization of CNTs

It is widely established in the literature that the end caps of nanotubes are more reactive than the side walls, owing to nanotubes' tendencies to form highly curved fullerene-like hemispheres at the tube ends. Hirsch stated in their research that sp<sup>3</sup>-hybridized defects, pairs of pentagon-

heptagons dubbed Stone-Walls defects, and voids in the nanotube walls are all regarded as defect locations for the tube ends and sides as seen in Figure 7 [57].

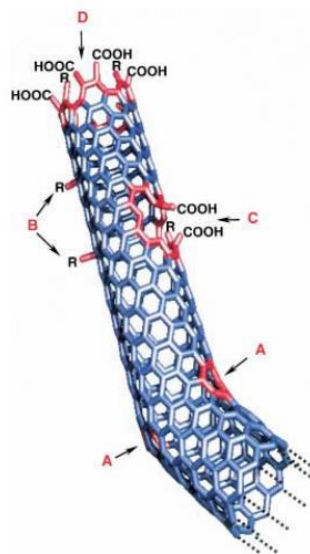


Figure 7 Typical Defects in a SWCNT [57]

Typical defects in a SWCNT include the following: A) five- or seven-membered rings in the C framework, rather than the conventional six-membered ring, which results in a bend in the tube; B) sp<sup>3</sup>-hybridized defects (R=H and OH); C) oxidative damage to the C framework, which results in a hole lined with -COOH groups; and D) an open end of the SWCNT terminated with -CO. Other terminal groups such as -NO<sub>2</sub>, OH, H, and C=O are also possible in addition to carboxy termini, which have been clearly confirmed.

Covalent functionalization of carbon nanotubes occurs at their end caps and/or sidewalls, while non-covalent functionalization includes mostly weak contacts between CNTs and commutative moieties, often along the CNT walls. Covalent surface modification refers to the chemical bonding of molecules having functional groups such as -COOH, -COH, and -OH to the sidewalls and termini of CNTs [58]. This process may take place through a variety of distinct reactions involving highly reactive chemicals. Chemical processes for fluorination, direct oxidation, amidation, radical addition and thiolation have been described in detail previously in the literature [58].

#### 2.4.1.1. Oxidation of CNTs

The most commonly employed surface modification procedures include the oxidation of CNTs using acids such as boiling nitric acid, a combination of sulfuric acid and nitric acid or "piranha" (sulfuric acid-hydrogen peroxide), or oxidative gases such as ozone [59]. Oxidative treatments

immediately bond carboxylic and other oxygen-bearing groups, such as hydroxyl, carbonyl, ester, and nitro groups, to the ends and/or defect sites in the side walls of CNTs (Figure 8). As a result of ozone oxidation, an ozonide group is formed as an intermediate that is subsequently converted to a secondary ozonide and/or other functional groups. The oxidation of CNTs causes the tube tip to open, the tube to shorten, and the sidewalls to break into acidic chemicals termed carboxylated carbon fragments. The extent to which these reactions occur, or the nanotubes' reactivity, is strongly dependent on their morphological characteristics, such as the curvature of the graphene within the tube, the tube diameter, and the tortuosity, defined as the ratio of the end-to-end distance ( $l$ ) to the contour length ( $l_0$ ), of the tube's outer graphene sheets [59].

All these features are defined by the parameters of the nanotube synthesis. Quantitative data defining the oxidatively surface-modified CNTs, such as the tube shape, diameter, and tortuosity of the tube's outermost graphene, might aid in developing tailor-made preparation techniques [59].

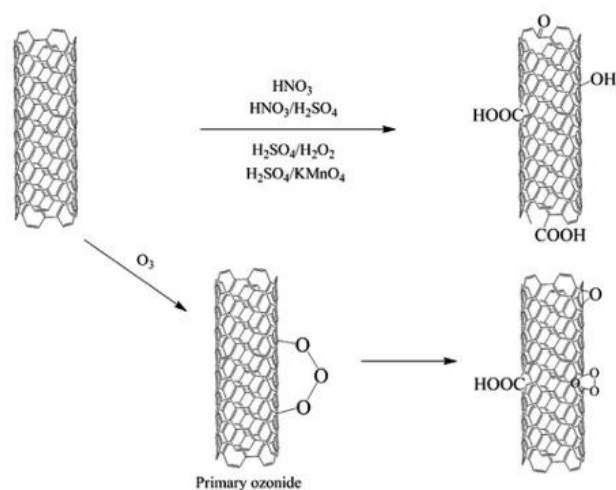


Figure 8 Scheme of procedure by the oxidation of CNTs by acid and oxidative gas [59]

To add carboxylic groups to the graphitic structure of MWCNTs, Xing et al. examined the oxidation of MWCNTs (95% purity, 30 nm in diameter) in a bath sonicated solution of equimolar  $\text{HNO}_3$  and  $\text{H}_2\text{SO}_4$ . Sonication was carried out for 1, 2, 4, and 8 hours. The treated MWCNTs were then centrifuged to separate them from the acids [60]. Prior to the structural investigation, functional MWCNT-COOH was washed and dried in vacuum. As a result, it was shown that a combination of sonication and acid treatments may be used to attach hydroxyl (OH), carbonyl (C=O), and carboxyl (COOH) groups.

By the deposition of several polar and non-polar functional groups onto CNT surfaces by covalent techniques, nanotubes can be made miscible in a variety of organic solvents. On the other hand, it is important to highlight that acidic oxidation opens the ends of nanotubes and creates a high number of defects on their sidewalls, resulting in carboxylated groups and, depending on the extent of the oxidation process, the fragmentation of CNTs into smaller pieces as shown in Figure 9 [61]. Although the acid oxidation of CNTs seems to be a simple chemical approach, the undesirable liquid waste created during solution-phase acidic oxidation of CNTs and the long purification procedures would significantly reduce their potential for large-scale commercial applications. As a result, alternative attempts have been made to design technologies that are easy to use, inexpensive, and cause the least amount of harm to the CNT structure and surroundings [56].

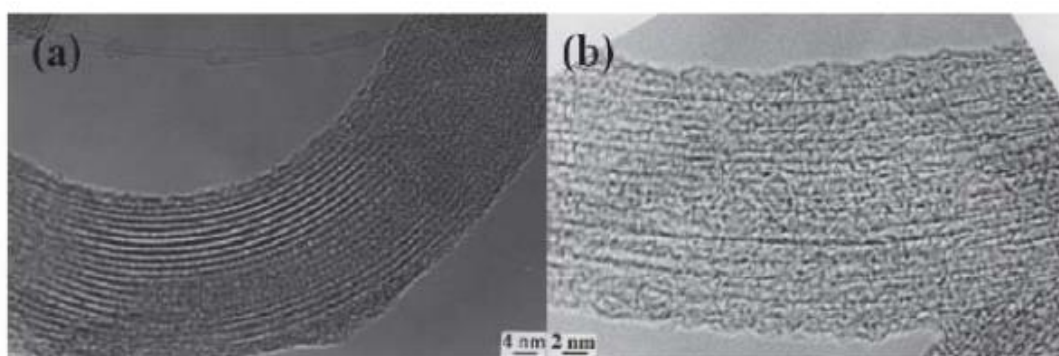


Figure 9 TEM images: (a) SWCNTs rope; (b) acid treated SWCNTs rope [61]

As an alternative to aggressive acidic treatment of CNTs for defect site functionalization, gas phase oxidation, more often referred to as "ozonolysis," stands out as the most effective surface modification technology in terms of being ecologically and economically friendly while having no detrimental impact on the carbon nanotube structure. Kim et al. demonstrated that ozone oxidation produces an intermediate ozonide group on carbon nanotubes, which later converts to secondary ozonide and/or other functional groups [58], as seen in Figure 8. Additionally, Banerjee et al. reported that the oxidative approach included three major characteristics: purification of SCWNTs to get a qualified product, chemical functionalization of nanotube sidewalls, and finally, systematic process development to achieve precise oxygenated functional group configurations. Finally, they generated carboxylic acids, aldehydes/ketones, or alcohols by post-reactions of primary ozonide species with hydrogen peroxide ( $H_2O_2$ ), dimethyl sulphide (DMS), or sodium borohydride ( $NaBH_4$ ), respectively [62].

### 2.4.1.2. Fluorination of CNTs

The surface modification of CNTs mainly refers to the modification of the sidewalls. The poor reactivity of sidewall surfaces, which are mostly composed of  $sp^2$ -hybridized carbons, makes chemical modification of CNT sidewalls difficult. Fluorination was one of the first sidewall functionalizations to be demonstrated directly. Under modest circumstances (fluorine's dissociation energy is just 38 kcal/mol), highly reactive F radicals may be produced, and fluorination retains the tubular form. The degree of fluorination is determined by the residual metal content in the catalysts used for CNT synthesis or by preparation conditions and treatment of carbon nanomaterial samples prior to fluorination (solvent type, annealing temperature) [63]. The degree of fluorination changes according to the reaction temperature from  $C_{3.9}F$  to  $C_{1.9}F$ [57]. Fluorinated carbon nanotubes (F-CNTs) provide a platform for the introduction of alkyl and/or aromatic groups through reactions with alkyl and/or aromatic peroxides (Figure 10) [63].

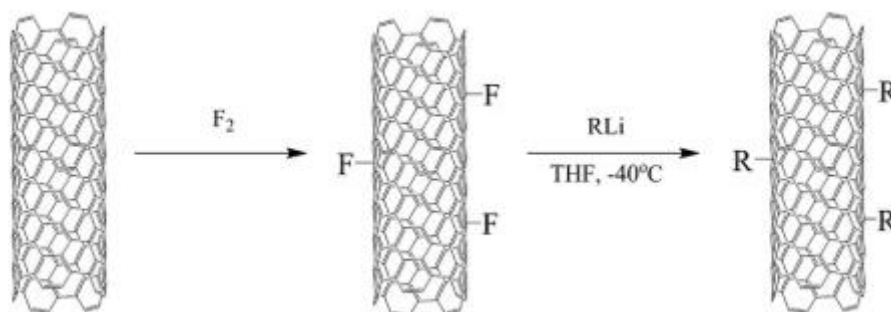


Figure 10 Schematic representation of CNT fluorination and subsequent alkylation [59]

### 2.4.1.3. Addition reactions

Addition reactions may be nucleophilic, electrophilic, or cycloadditional. For instance, as seen in Figure 11, a nucleophilic dipyrityl imidazolidene may combine with the electrophilic SWCNT p-system to form zwitterionic polyadducts [64]. CNTs have a negative charge because one negative charge is transferred from the imidazolidene to the delocalized CNT surface. This is similar with the nucleophilic addition findings obtained with  $t\text{-BuLi}$  [65]. Due to electrostatic repulsion, negatively charged CNTs disperse uniformly in solution. Nucleophilic addition introduces a novel way for doping CNTs, allowing for the modification of their electrical characteristics. SWCNTs may be utilized to add surface modifiers through the reaction with  $CHCl_3$  in the presence of  $AlCl_3$  chlorine. After the hydrolysis of the labile chlorinated intermediate species, hydroxy-functionalized SWCNTs were formed (Figure 12) [66].

Microwave irradiation may aid in the electrophilic addition of alkyl halides to CNTs [58]. Cycloaddition is one approach for altering the surface properties of CNTs. As seen in Figure 13, an aziridine ring was formed on the CNT surface through [2 + 1] cycloaddition of nitrenes [64]. [2 + 1] cycloaddition of nitrenes resulted in the formation of crosslinks between CNTs [67] and a significant improvement in their solubility in organic solvents. Raman and UV/VIS/NIR absorption spectra demonstrated that SWCNTs retained their electronic characteristics after the surface modification [68]. As a result, just a few flaws were introduced in the CNT surface to enable surface modification and covalent bonding. Dichlorocarbene addition is another approach to generate cyclopropane on the surface of CNTs, since dichlorocarbene is an electrophilic reagent that adds to the deactivated double bond [58].

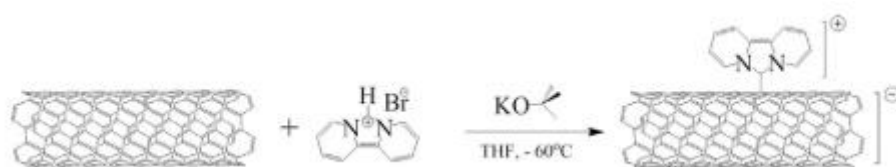


Figure 11 Schematic representation of nucleophilic addition of dipyrindyl imidazolide to CNTs [59]

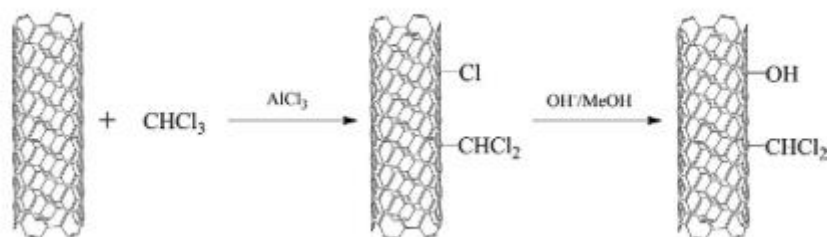


Figure 12 Schematic representation of the electrophilic addition of  $\text{CHCl}_3$  to CNT and hydrolysis of the functionalized CNTs [59]

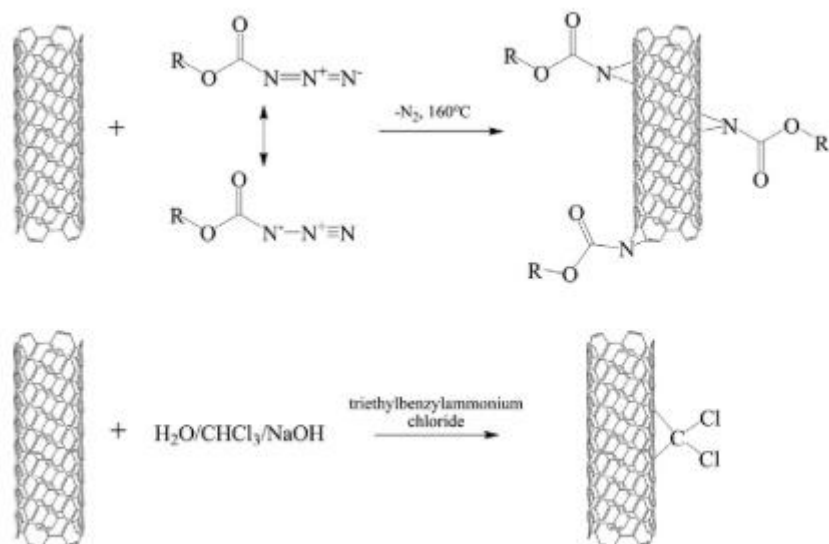


Figure 13 Schematic representation of [2 + 1] cycloaddition of nitrenes and the dichlorocarbene addition [59]

#### 2.4.1.4. Radical addition

Using aryl radicals generated from diazonium salts, aryl groups may be bonded to the surfaces of CNTs. Aryl radicals may react electrochemically with CNTs using buckypaper as the working electrode, or they may react with the equivalent anilines to modify CNTs in a few different ways [58]. The addition of aryl radicals to CNT surfaces enables 'solvent-free modification' [69]. In polymer matrixes, solvent-free modification results in highly functionalized and dispersible nanotubes. Surfactants and aryl diazonium salts may be used to modify individual nanotubes (Figure 14). The tubes that arise stay unbundled throughout their lengths and are incapable of re-agglomerating. This procedure results in a high degree of surface modification, up to one in nine carbons on a nanotube, and highly dispersible CNTs in DMF or aqueous solutions [70].

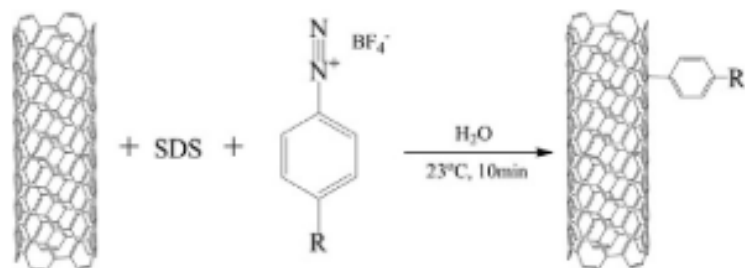


Figure 14 Schematic representation of the radical addition of diazonium salts to CNTs [59]

#### 2.4.1.5. Thiolation reactions

Thiol groups have a remarkable affinity for metal surfaces, most notably gold [71]. Thiolation of CNTs is a critical step in the preparation of CNT–metal composites. Kim et al. accomplished thiolation of CNTs as seen in Figure 15 [72]. Carboxylic groups introduced during the oxidation processes may be transformed to thiol groups by reducing them to methylol groups with  $\text{NaBH}_4$ , chlorinating them to methyl chloride with  $\text{SOCl}_2$ , and then thiolating the methylol groups with  $\text{H}_2\text{S}/\text{NaOH}$ . By using Au–S chemical bonding, the thiolized tubes may subsequently be constructed as monolayers on a gold surface.

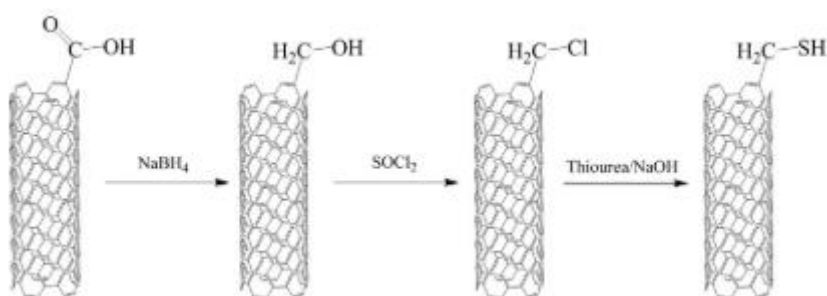


Figure 15 Schematic representation of the thiolation of CNTs [59]

#### 2.4.2. Non-covalent surface modifications of CNTs

The benefit of the non-covalent surface modification method is that the  $\text{sp}^2$  hybridization is retained inside the graphitic structure of CNTs, preserving their electrical characteristics while substantially increasing their solubility. The technique of non-covalent chemistry is based on the adsorption of molecules onto the surfaces of CNTs, a process known as wrapping [73].

Through stacking interactions, surfactants, amphiphilic copolymers, and polyaromatic compounds can be adsorbed onto the surfaces of nanotubes. As a result, non-covalent functionalization is regarded as the simplest and the most successful method for increasing the miscibility and solubility of CNTs without causing disruptions in the nanotubes' primary graphitic structure. Surfactants, for example, are utilized since their hydrophilic ends interact with polar solvent molecules while their hydrophobic ends adsorb onto the surfaces of nanotubes [74]. Thus, the length of the surfactant's hydrophobic regions and the type of hydrophilic groups play a critical role in dispersing nanotubes separated from bundles, aggregates, or ropes in organic solvents [59]. In another instance, the aggregation behaviour of

CNTs in a solvent can be significantly decreased by adsorbing surfactant molecules onto the sidewalls of the nanotubes, reducing the surface tension and enhancing the wettability and adhesion properties of them. Additionally, non-covalent functionalization may overcome strong van der Waals interactions between nanotubes through electrostatic or steric repulsive forces. The surfactant characteristics, the medium chemistry, and the polymer matrix all have a significant role in determining the effectiveness of this modification technique [73]. Sodium dodecyl sulfate (SDS), lithium dodecyl sulfate (LDS), and sodium dodecylbenzene sulfonate (SDBS) are some of the most straightforward and widely utilized surfactants for non-covalent functionalization and dispersion of CNTs. It is worth noting, however, that the adsorption of tiny surfactant molecules onto CNTs may potentially have a detrimental effect on the mechanical properties of end products such as polymeric composites. On the other hand, polymers, particularly conjugated polymers, have been demonstrated to be excellent wrapping materials for non-covalent functionalization of CNTs due to the  $\pi$ -stacking and van der Waals interactions between the conjugated polymer chains containing aromatic rings and the carbon nanotube surfaces [75].

## **2.5. Silane coupling agents**

Plato initially proposed the idea of two distinct components being kept together by a third intermediate substance acting as a coupling agent to explain how a world made up of four elements — earth, air, fire, and water – could exist as a unified entity [76]. Coupling agents have long been regarded to be crucial in the growth of the use of polymeric structural materials in various sectors [76]. They are used to increase the adhesion and compatibility of diverse and different materials. Because they include two separate functional groups—one that is attracted to the polymeric matrix and the other that is absorbed by the surface of the filler—a broad variety of coupling agents are effective for this purpose [77]. The coupling agent, according to Tan et al. [78], acts as a "molecular bridge" across the interface of different polymer binder and fillers, resulting in the creation of covalent connections across the interface, which enhances the composite system's characteristics.

When glass fibers were initially utilized as reinforcement in organic resins in 1940s, there was an immediate need for novel bonding processes [76]. The use of silane coupling agents in coating applications to promote adhesion between inorganic surfaces and polymeric molecules has been recommended in many research studies since then [79]. They were studied as coupling agents to promote the adhesion of organic polymers to mineral surfaces like glass fibers in

composites because they are hybrids of silica and organic compounds linked to polymers [76]. Silane coupling agents have three key advantages:

- (i) they are commercially accessible in large quantities,
- (ii) they contain alkoxy silane groups capable of interacting with OH-rich surfaces on one end, and
- (iii) they contain a wide range of functional groups that can be tuned based on the matrix to be employed on the other end.

Coupling agents' primary function is to increase the adhesion, which leads to changes in resulting composite structures' mechanical and electrical characteristics such as tensile and flexural strength, fracture toughness, tensile modulus, bulk electrical characteristics, dielectric coefficient, and so on [76], [80].

Demjen et al. discovered that silane compounds with various functional groups affected the mechanical characteristics of PP/Caco3 composites in various ways [81]. Ralph K. Witt discovered in 1947 that allyltrimethoxysilane on glass fibers produced polyester composites with double the strength of those made with ethyltrichlorosilane-treated glass [82]. Kaynak et al. [83] investigated several silane coupling agents to increase the interfacial bonding between recycled rubber particles and the epoxy matrix. Tezvergil et al. verified that using silane as a regular treatment promoted the adhesion between polymeric matrix and fibers [84]. The 'bridging effect' between high density polyethylene and silane modified TiO<sub>2</sub> was found by Hashimoto et al. [85]. A plasticizing effect was seen at high silane loading levels, with impact strength decreasing [86]. By lowering polymer viscosity, Hashimoto et al. reported that utilizing silane coupling agents enhances the entry of polymer into the voids between the reinforcing agent of a matrix [85].

In recent years, silane coupling agents have been employed to modify the surface of nanofillers in polymeric matrixes. Tee et al. used silver nanoparticles as a filler in an epoxy nanocomposite with silane, and the nanoparticle dispersity, electrical, and flexural characteristics of the composite improved dramatically [77]. Cheng et al. utilized a silane sizing on CNTs to activate the surface and increase its adherence to epoxy as depicted in

Figure 16 [7].

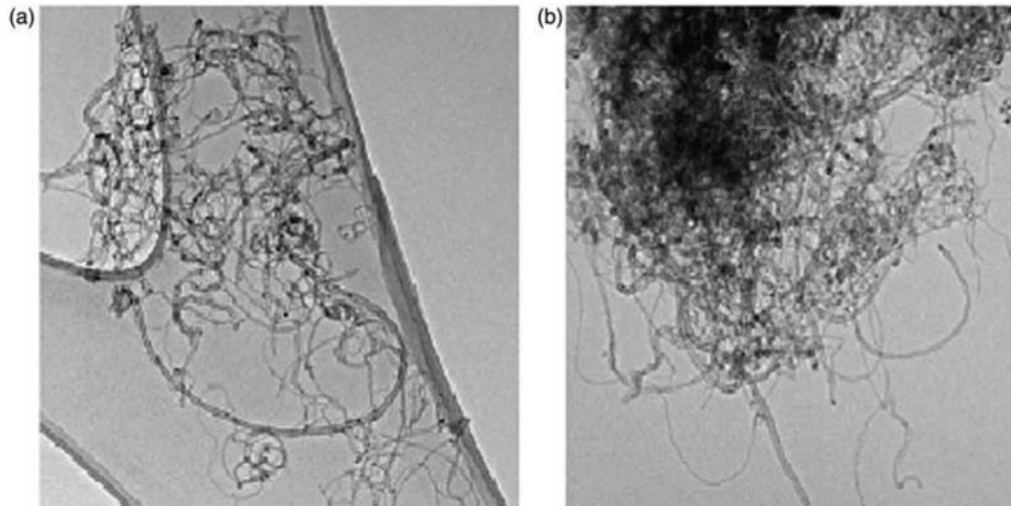
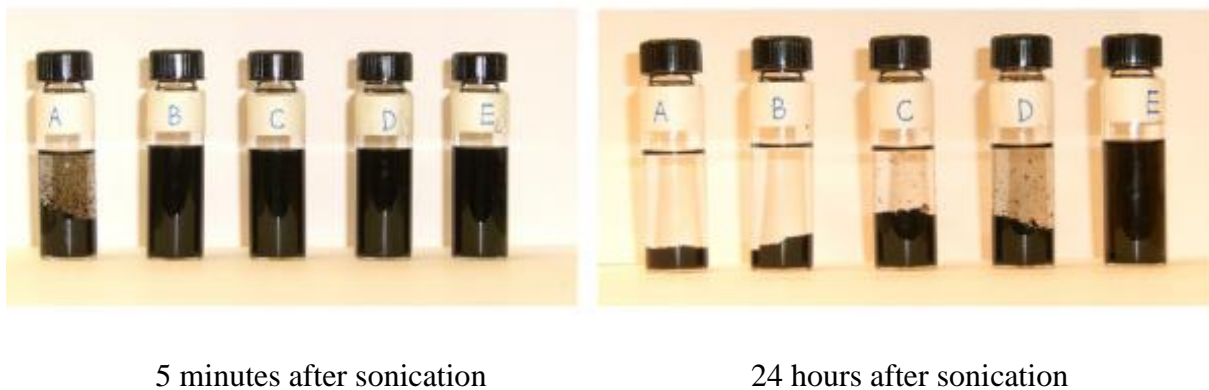


Figure 16 a) Silanized CNT b) Pristine CNT [87]

According to Peng et al., the suspension stability of CNTs treated with silane compounds is much greater than that of pristine or other modified samples (Figure 17) [87].



5 minutes after sonication

24 hours after sonication

Figure 17 Suspension stability of the MWCNTs (A: Pristine, B: Pretreated, C: UV/O<sub>3</sub>-treated, D: Reduced, E: Silanized) [87]

### 2.5.1. Coupling mechanisms of silane compounds

Silane coating agents are compounds that serve to form durable chemical bonds between the surfaces of two different types of materials. They are generally used to hold an organic material and an inorganic material together. These compounds are designed to contain at least two different functional groups to hold two different materials together [1]. Durable chemical bonds established between two different structures significantly increase the mechanical and chemical resistance and adhesion properties of resulting composite or hybrid materials. They are highly effective chemicals for adjusting the desired properties by combining two materials with

different physical and chemical properties and adding new properties to the materials [2]. They can also be used to solve problems such as difficulties in the dispersion of hydrophobic materials in water with the help of different functional groups. Organosilanes are one of the frequently preferred coating agents in these applications. Their general structures are shown in Figure 18. They contain a functional end (R) compatible with organic materials and another end compatible with inorganic materials in a single molecule. X is a hydrolyzable group such as alkoxy or halogen [3].

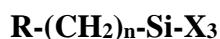


Figure 18 General formula of silane coupling agents

Most commonly used organosilanes have three hydrolyzable groups and one functional group, although these numbers may vary. The higher the number of hydrolyzable groups (X), the higher the degree of bonding.

Alkoxy groups attached to the silicon atom form silanol structures by hydrolysis in water, and they both form strong covalent bonds with the surface and polymerize within themselves by undergoing a condensation reaction with hydroxyl (-OH) groups on the surface of substrates and/or silanol groups within themselves (see Figure 20) [3]. Bonding to the CNT surface can be achieved in this way. R functional ends can be amine, isocyanate, epoxy, etc. to be compatible with the desired material. They can be covalently bonded with organic materials by designing with proper functional groups (Figure 19).

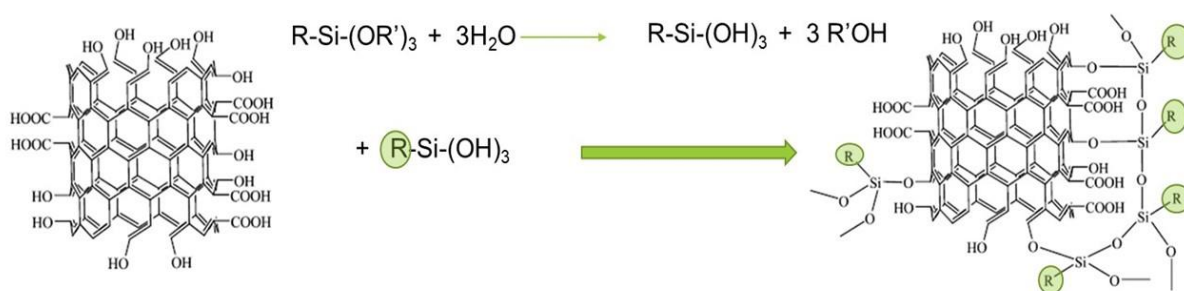


Figure 19 Reaction mechanism of trialkoxy organosilane compounds to the carbon nanotube surface

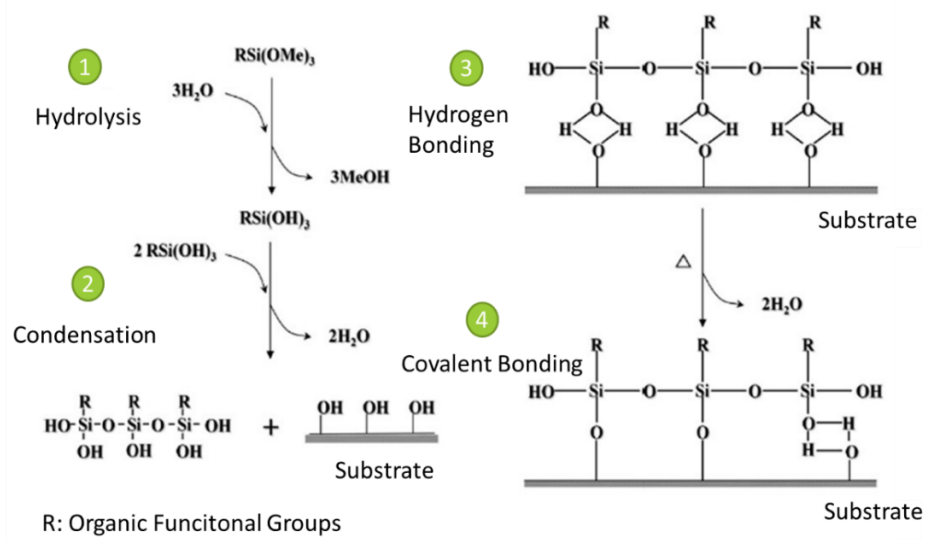


Figure 20 Coating mechanism of alkoxy silane compounds with sol-gel method

## CHAPTER 3

### 3. FUNCTIONALIZATION, DISPERSION AND ULTRASONIC SPRAY DEPOSITION OF CNTs

#### 3.1. Materials

SWCNTs with a purity of > 93 wt.% (average diameter of 2 nm and length of 5 micron) were kindly provided by OCSiAl. N-[3-(Trimetoxysilyl)propyl] ethylenediamine with a purity of >97% and ethanol with a purity of >99% were purchased from Sigma-Aldrich. 1,3-Propanesultone with 99% purity was purchased from Alfa Aesar.

#### 3.2. Ozonolysis of CNTs

The surface oxidation of SWCNTs was achieved by continuously flowing ozone gas produced by an ozone generator (A2Z Ozone Systems Inc.) through a vertical column packed with dry SWCNTs. Excess ozone gas passed through the vertical reactor is trapped in a glass Erlenmeyer filled with sodium iodide solution. Schematic of ozone oxidation setup is seen in Figure 21. Ozone gas was fed through the vertical reactor at room temperature with a flow rate of 4 L/min. Different SWCNT oxidation studies were carried out as a function of varying oxidation times.

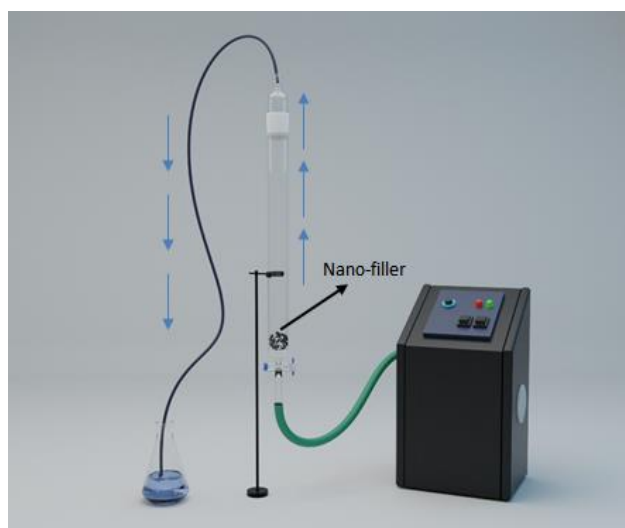


Figure 21 Ozone Oxidation Setup

#### 3.3. Design of a novel, multi-functional silane coupling agent

Commercially available silane coupling agents can be further modified to achieve additional functionalities. The two main features aimed in this study were to obtain good dispersion of the functionalized CNTs in water and the strong bonding of the CNTs with the epoxy matrix and/or fiber surfaces. In this context, one end of the new silane coupling agent was designed to be an

inorganic functional group that will bond with the CNT surface or fiber surface, whereas the other end was designed to render not only hydrophilicity but also ability to form covalent bonds with epoxy resin, an organic thermosetting polymer. While silanes with alkoxy functional groups were used for this purpose, the other end of the chain was designed as an amino-functional zwitterionic group (Figure 22).

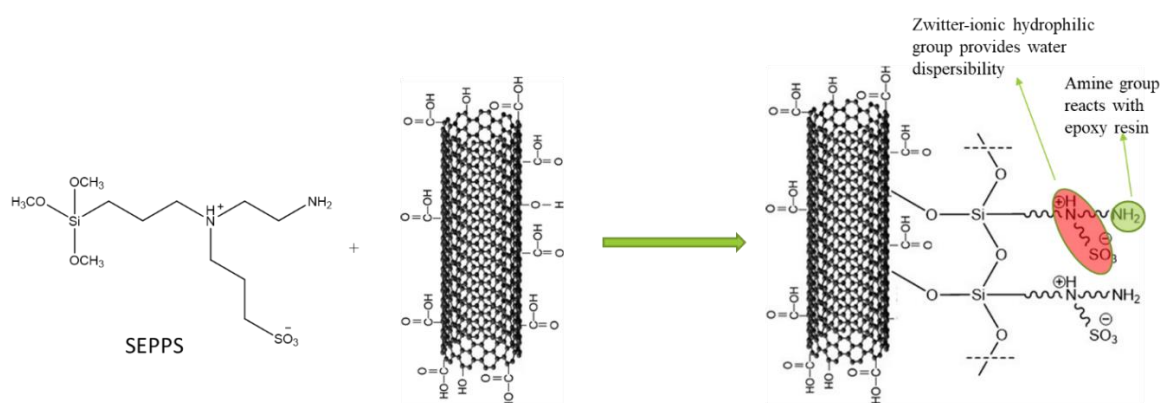


Figure 22 Reaction of SEPPS with oxidized CNT

### 3.3.1. Synthesis of 3-((2-aminoethyl) (3-(trimethoxy silyl) propyl) ammonium) propane - 1-sulfonate (SEPPS)

The newly synthesized SEPPS coupling agent is a multifunctional coupling agent containing both a primary amine group and a zwitterionic group, obtained as a result of the reaction of alkoxy silane with diamine functional group with 1,3-propanesultone (Figure 23). While the zwitterionic part greatly facilitates dispersion in water, the secondary amine group on the same group enables the bonding of CNTs to epoxy to form the epoxy-CNT bridges (see Figure 22). The reaction was carried out in dry acetone and nitrogen atmosphere at room temperature.

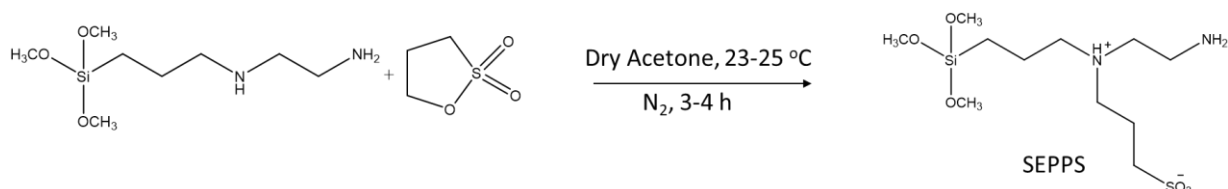


Figure 23 Schematic of SEPPS synthesis

### **3.4. Preparation of SEPPS incorporated SWCNTs**

#### **3.4.1. Preparation by chemical reaction**

Oxidized SWCNTs were sonicated in ethanol-water solution (%95 EtOH) for 1 hr. In the meantime, solid SEPPS was dissolved in a separate ethanol-water solution (%95 EtOH). At the end of the sonication process, SEPPS solution and SWCNT dispersion were added into a round bottom flask which was equipped with a condenser. The reaction was allowed to continue at 70°C for 4 hr in an oil bath. After 4 hr of a reaction, SEPPS functionalized SWCNTs were filtered through 0.45-micron pore size PTFE membrane filter and rinsed with deionized water several times to get remove excess, unreacted SEPPS on SWCNT surface. For the final dispersion, rinsed SWCNTs were dispersed in deionized water by sonication.

#### **3.4.2. Preparation by physical mixing**

Oxidized SWCNTs were sonicated in deionized water for 1 hr. In the meantime, solid SEPPS monomers were dissolved separately in deionized water. After the sonication, SEPPS solution was added into a beaker which containing sonicated oxidized SWCNTs and a physical mixture of SEPPS and SWCNT was obtained. In this process, different from the chemical reaction approach, no rinsing was performed to enable the hydrolysis of SEPPS compounds on the fiber fabric upon ultrasonic spray deposition and to form a crosslinked siloxane network with bonding between fiber surface-SWCNTs-epoxy matrix, which is expected to increase mechanical properties of the final composite.

### **3.5. Dispersion of SEPPS incorporated SWCNTs**

In this study, solvent-free, environmentally friendly SWCNT dispersions were obtained from chemically modified SEPPS-SWCNTs and physically mixed SEPPS-SWCNTs in water with the aid of a probe sonicator (SONICA Q700 equipment) operated at 80% amplitude with 5 seconds pulse on and 5 seconds pulse off.

### **3.6. Ultrasonic spray deposition of SWCNTs**

SONO-TEK INC. ExactaCoat ultrasonic spray coater was utilized for deposition of SEPPS incorporated SWCNTs samples onto fiber surfaces as seen in Figure 24. This approach enables coating large areas without the need of fillers or stabilizers by spraying the loaded solution onto a substrate using an ultrasonic nozzle. It is used in conjunction with an ultrasonic syringe to maintain an uniformly sprayed solution throughout the procedure, preventing the suspension's flakes/particles from settling. After loading the suspension into the syringe, it is sonicated as it

is injected into the nozzle. The nozzle's ultrasonic vibration oscillates the suspension within, generating capillary waves. When these waves reach the nozzle's atomising surface (tip), they gain an amplitude high enough to separate off the surface, generating the spray. The size of the droplets is determined by the frequency of the ultrasonic vibrations, which exhibit an inverse linear relation. A 48 kHz impact ultrasonic spray shaping nozzle was utilized for this experiment. A jet air deflection system powered by compressed air gas is then used to guide the spray onto the substrate. The gas supply aids in the structuring of the spray and does not entail the suspension being pushed as with a normal pressure spray. The cloth substrates were placed on a hot plate heated to 50 °C to remove any remaining moisture.

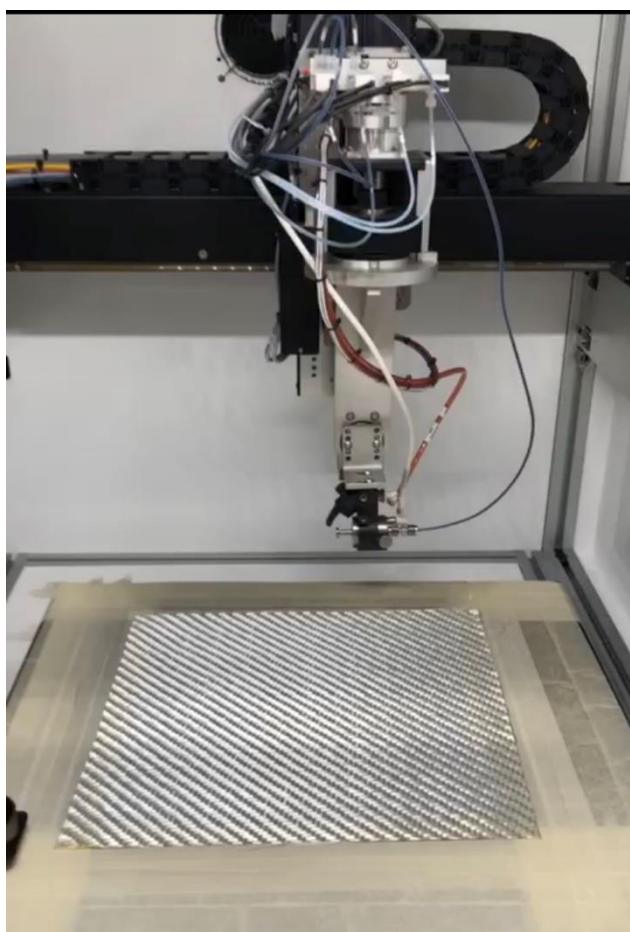


Figure 24 Ultrasonic spray deposition of SEPPS-SWCNT aqueous dispersion on glass fiber fabric

### **3.7. Results and Discussion**

#### **3.7.1. Thermogravimetric analysis of oxidized SWCNTs**

Thermogravimetric analysis (TGA) of selected samples was conducted with the Shimadzu DTG60H Simultaneous DTA-TG equipment. Analyses were performed between 30 °C and 1000 °C at a heating rate of 10 °C/min under a nitrogen flow rate of 100 ml/min.

TGA studies of pristine and oxidized SWCNT samples were conducted as a function of ozone treatment time. As shown in Figure 25, oxidized nanotubes showed mass loss over three distinct temperature ranges. The water or moisture on the nanotube surface evaporated firstly around 100°C, whereas organic compounds such as carboxylic acid and hydroxy group are expected to decompose between 100 - 300°C. Although mass loss for pristine SWCNTs was negligible at these temperatures, weight losses of up to 15% was obviously seen in oxidized SWCNTs, particularly in the second region. Additionally, the mass loss between 100-300°C increases with increasing ozone treatment duration, indicating that the hydroxy and carboxylic acid groups increase proportionally as a function of the ozonolysis reaction time.

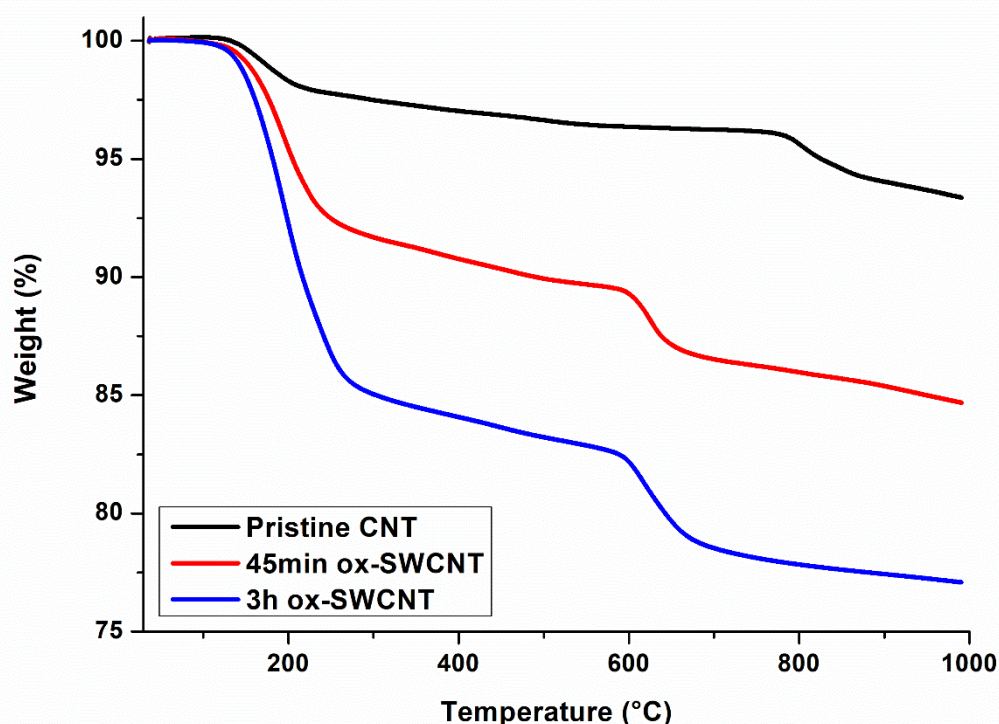


Figure 25 TGA results of oxidized SWCNTs.

A series of TGA analyses was also conducted to demonstrate that the oxidized SWCNTs were covalently bonded to SEPPS and that the SWCNTs were successfully functionalized. As shown in the Figure 25, while the -OH and -COOH groups of oxidized SWCNTs decomposed between 100 and 300°C, when Figure 26 was analysed, the absence of mass loss in the chemically modified SEPPS-SWCNTs between 100 and 300°C demonstrates that the -OH and -COOH groups of the oxidized SWCNTs were successfully converted. When the TGA graph of SEPPS is examined, the decomposition temperature is found to be about 400 °C. Thus, the mass loss of chemically modified SEPPS-SWCNTs around 400 °C indicates that the functionalization with SEPPS is effective. Additionally, the degree of the functionalization of SWCNT with

SEPPS increased systematically with increasing amount of SEPPS during the chemical modification as indicated by SWCNT:SEPPS weight ratio varying from 1:1 to 1:20. When the CNT:SEPPS ratio was increased from 1:1 to 1:10, the mass loss at 400 °C rose by about 9%. When it was increased from 1:1 to 1:20, mass loss increased by 18%.

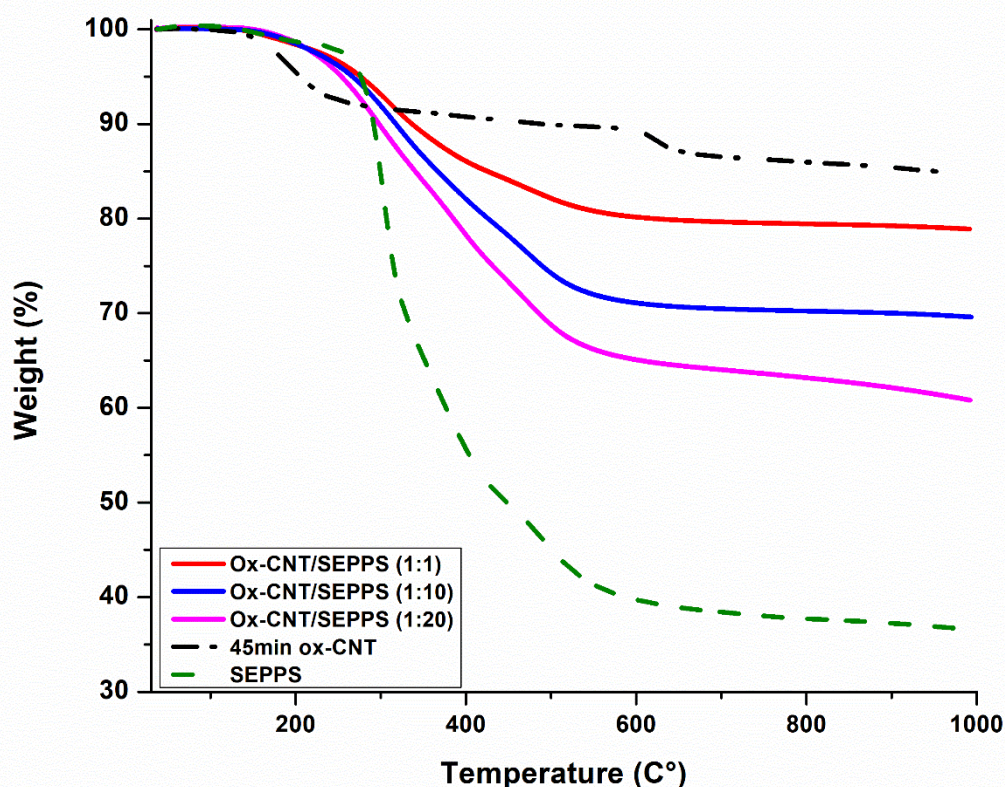


Figure 26 TGA results of chemically modified SEPPS-SWCNTs

### 3.7.2. X-Ray Photo-Electron Spectroscopic (XPS) analysis

XPS is a useful method for determining the elements and type of bonds present on a surface. XPS analysis is accomplished by blasting a photon at a sample. Einstein's photoelectric effect states that an electron is emitted from a surface. This electron's binding energy ( $E_b$ ) is measured and studied. Each element has a unique  $E_b$ . As a result, XPS may be used to determine the elemental composition of the surface. Additionally, depending on the take-off angle, it delivers information on the chemical surface with a spatial resolution of a few millimeters and a depth resolution of 5 nm [88].

Along with TGA data, the XPS method was employed in this work to determine the elemental composition of nanotubes and to conduct a more complete assessment of the effect ozone oxidation. In Figure 27, an increase in O1s peaks on the surface of SWCNTs was detected as the ozonation duration increased. The findings of the XPS study are consistent with those of the TGA study. The formation of oxygen-containing groups on the surface is found to rise systematically with the ozonation period.

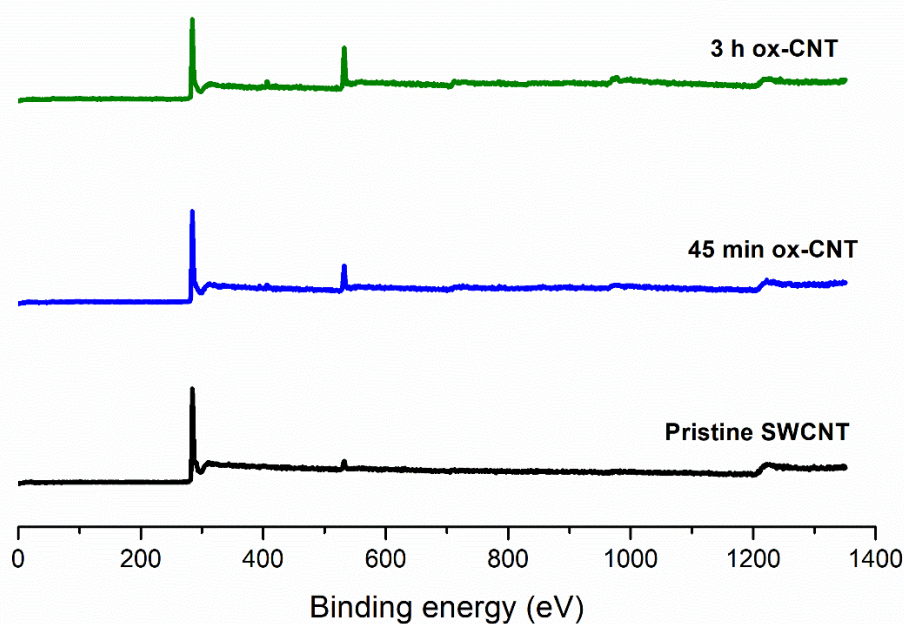


Figure 27 XPS results of pristine, and ozone treated SWCNTs

### 3.7.3. Dispersion of SEPPS-SWCNTs

Aqueous SWCNT dispersions studies were carried out for two different samples: (i) chemically modified SEPPS-SWCNTs and (ii) physically mixed SEPPS-SWCNTs. Both dispersions were first visually inspected. As seen in Figure 28 the dispersions prepared by the chemical modification of SWCNTs with SEPPS formed large agglomerations and could not be dispersed homogeneously in water. Since the nanotubes that could not be dispersed homogeneously could not be sprayed properly onto the fiber surface by ultrasonic spraying, the study was continued with physically mixed SWCNTs with SEPPS.

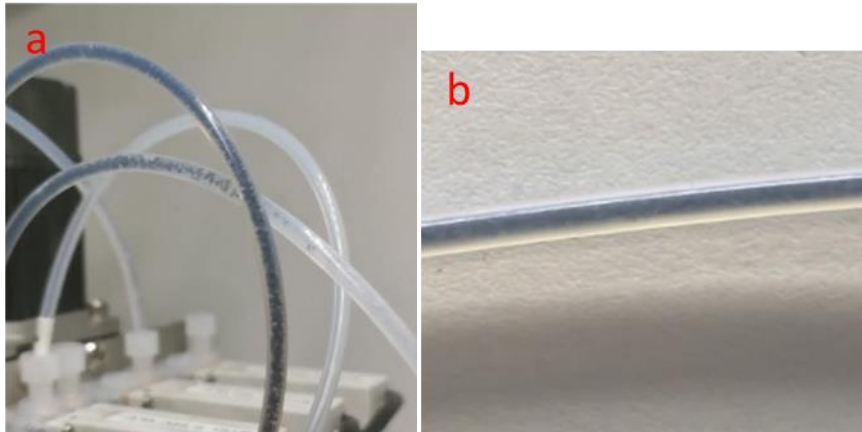


Figure 28 SWCNTs in water a) after reaction with SEPPS b) after physical mixing with SEPPS

Particle size measurements were used to evaluate the dispersion of SWCNTs physically mixed with SEPPS in water (Figure 29). To begin with, pristine SWCNTs were dispersed for 30 minutes by probe sonication in water. Secondly, SWCNTs which were oxidized by ozone treatment were dispersed in water using probe sonication for the same period of time. Finally, oxidized SWCNTs that were combined with SEPPS 1:1 and 1:2 ratios and dispersed in water using probe sonication for 30 minutes. Concentrations of all dispersions were set to 0.05 wt% in water. The particle sizes of SWCNTs in four different dispersions were determined immediately after sonication. Pristine SWCNTs were found in the form of huge agglomerations in water, with a broad, multi-modal particle size distribution. The average diameter of pristine SWCNT particles in water was measured to be 1000 microns. Upon the ozone treatment of pristine SWCNTs, a significant improvement was observed in their dispersion characteristics. While large-scale agglomerations continued to be present, the average particle size of the majority of particles has decreased from 1000 microns to approximately 100 microns. On the other hand, it was noted that SWCNTs physically mixed with SEPPS had a more defined particle size distribution and smaller particle sizes and variations. In water, the average diameter sizes of the particles were measured to be approximately 30 microns for those physically mixed with SEPPS in a 1:1 ratio. When the amount of SEPPS was doubled in the mixture, the average particle size further decreased, demonstrating that physical aqueous mixtures of the designed silane coupling agent with SWCNTs could be suitable for delivery onto fiber surfaces by ultrasonic spray deposition.

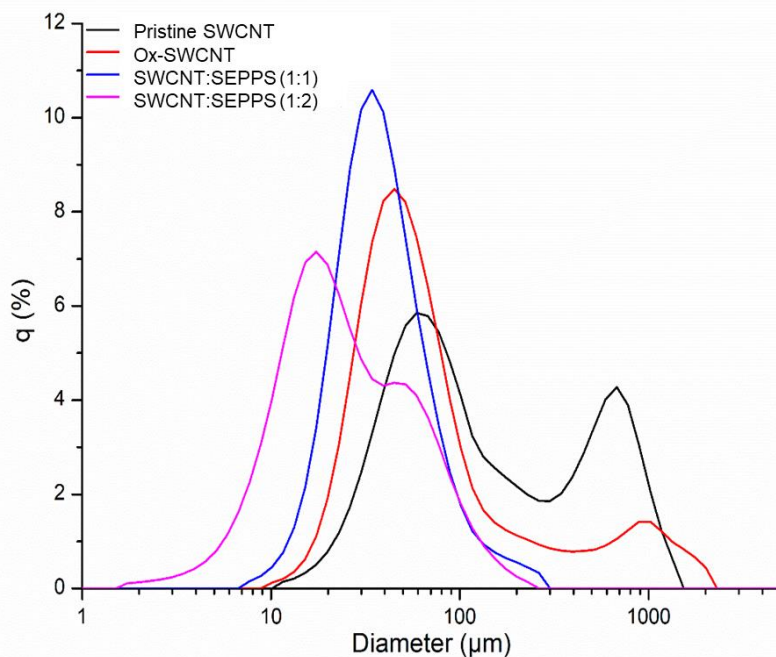


Figure 29 Particle Size Measurements of pristine, oxidized and SEPPS-SWCNTs physically mixed.

### 3.7.4. Scanning Electron Microscope (SEM) analysis

Once a homogeneous dispersion and distribution of nanotubes was ensured and maintained in water, they were deposited onto fiber surfaces by ultrasonic spray deposition. SEM was used to assess the surfaces of SWCNT deposited glass and carbon fiber mats prepared under various conditions. A Leo SUPRA 35VP FEG-SEM device was used to evaluate the surface morphology of the samples. Three distinct concentrations of pristine, ozonated, and physically mixed SEPPS-SWCNTs were sprayed onto the surface of the glass fiber using an ultrasonic spraying technique, and SEM pictures were captured.

As shown in the particle size measurements, since pristine SWCNTs were unable to maintain a uniform particle distribution in water, they immediately blocked the pipes and the pump of the ultrasonic spraying device due to massive agglomerations rendering the device incapable of spraying. As it has been found that oxidized SWCNTs were more uniformly dispersed than pristine nanotubes, and that agglomerated structures were smaller than pure structures they were successfully deposited on glass fiber fabric surfaces. Yet, as seen in Figure 30, the distribution of SWCNTs that were physically mixed with SEPPS was considerably more homogenous in compared to oxidized SWCNTs. Additionally, individual nanotubes have been found to be

easily distinguishable, with almost negligible agglomeration in the physically mized SEPPS-SWCNT sample. Given the bridges formed between the fibers, it was presumed that SWCNTs in the presence of the multi-functional silane coupling agent SEPPS might enhance the surface area of glass fibers and improve the wetting and adhesion with epoxy resin during the manufacturing of FRPCs.

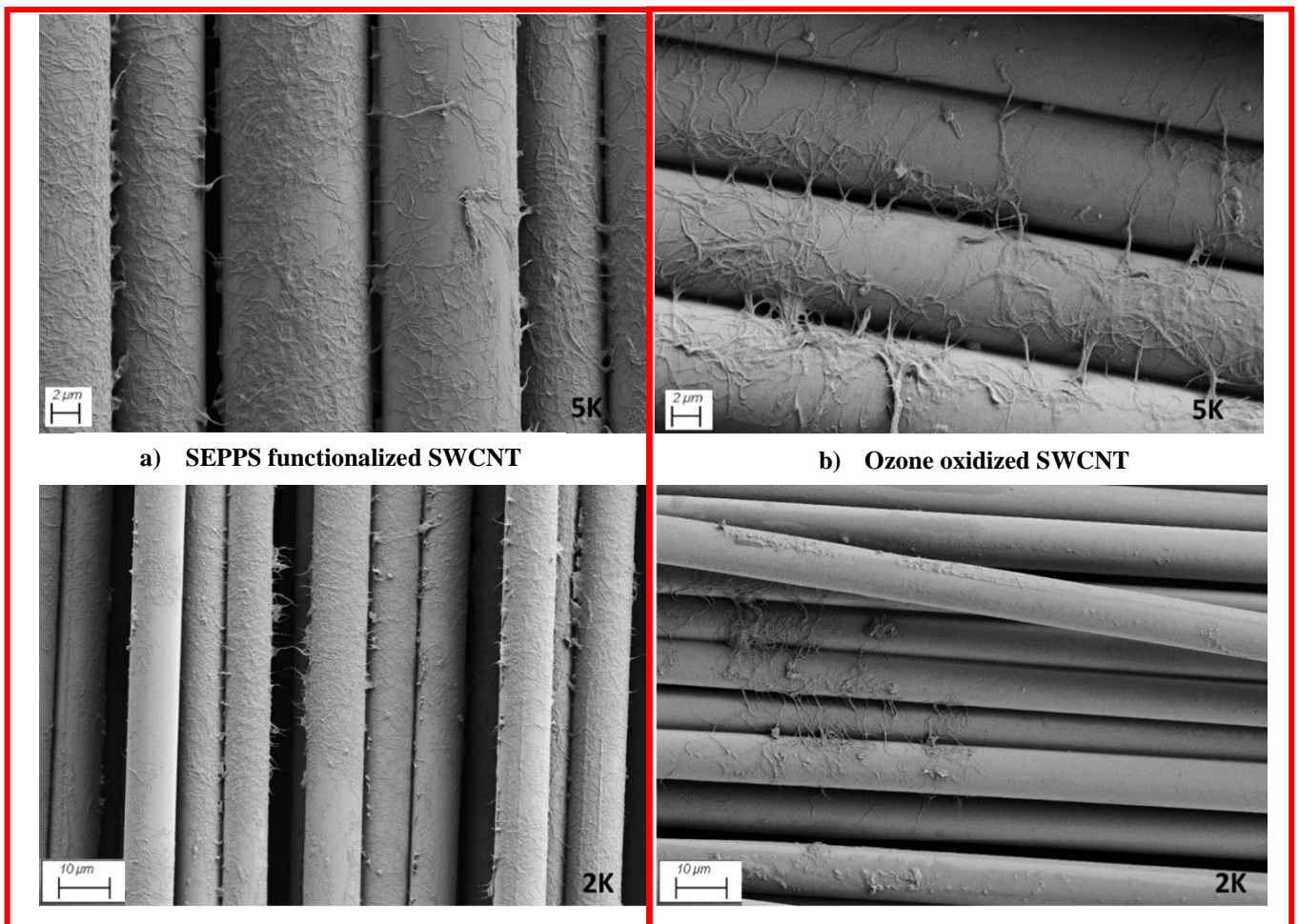


Figure 30 SEM images of a) SEPPS-SWCNT b) oxidized-SWCNTs sprayed onto glass fiber fabric by ultrasonic spray deposition

### 3.8. Conclusions

The presence of -OH and -COOH groups on SWCNT surfaces upon the treatment of a continuous ozone gas flow demonstrated that the oxidation of nanotubes was successful. Additionally, the degree of functionalization on the SWCNT surface increased systematically as a function of the ozonolysis duration as evidenced by TGA and XPS.

Considering the dispersion quality of prepared SWCNTs in water by visual inspections it was clear that the chemical modification of SWCNTs with SEPPS was not satisfactory to obtain

agglomerate-free, homogeneous dispersions. On the other hand, physical mixtures of SWCNTs with SEPPS in water yielded homogeneous dispersions with significantly lower and more uniform particle sizes. Possible reasons for the dispersion quality of both samples were depicted in Figure 31.

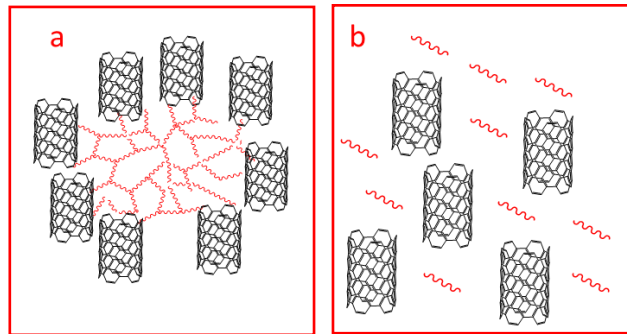


Figure 31 Demonstration of SWCNTs in water a) after reaction or b) after physical mixing with SEPPS

Detailed studies revealed that a sonication duration of 30 min and a SWCNT concentration of 0.05 wt% was suitable to achieve a homogenous and stable dispersion in water. SEM analyses revealed that ultrasonic spray deposition of obtained SEPPS-SWCNTs dispersions enabled the homogeneous coverage of fiber surfaces with distinct nanotube bridges between individual fibers, demonstrating that sprayed SWCNT dispersions pose a huge potential for the improvement of the mechanical properties of resulting FRPCs as reported in Chapter 4.

## CHAPTER 4

### 4. PRODUCTION and CHARACTERIZATION of FRPCs CONTAINING CNTs

#### 4.1. Materials

SWCNTs with a purity greater than 93 wt.% (average diameter of 2 nm and length of 5 micron) were kindly provided by OCSiAl. Glass fiber fabric was unidirectional Metyx LT 450 E10A. SEPPS was previously synthesized in-house as described in Chapter 3. Biresin CR80 epoxy resin and Biresin CH80-10 hardener were purchased from Sika group.

#### 4.2. Preparation of aqueous SWCNT dispersions

Oxidized SWCNT samples (Ox-SWCNT) samples that were prepared by ozone oxidation described in Chapter 3 were ultrasonically treated under probe sonication (SONICA Q700 equipment) in deionized water for 1 hour under 80% amplitude with 5 seconds pulse on and 5 seconds pulse off. Meanwhile, solid SEPPS monomers were dissolved in deionized water. After the sonication, SEPPS solution was mixed into the beaker containing the sonicated, oxidized SWCNTs. Lastly, the final dispersion was further subjected to ultrasonication under the same conditions above. Two different SEPPS-SWCNT dispersions with ratios of 1:1 and 2:1 by weight, respectively, were prepared by physical mixing. SWCNT concentration was 0.05 wt% in each dispersion. As a control, only Ox-SWCNT aqueous dispersion and SEPPS aqueous solutions were also prepared.

#### 4.3. Spray deposition of aqueous SWCNT and SEPPS/SWCNT dispersions onto glass fiber fabrics

Nanomaterials were sprayed on glass fiber surfaces using a SONO-TEK Inc ExactaCoat ultrasonic spray coater using a 48 kHz impact ultrasonic spray shaping nozzle. The spray is guided onto the substrate using a jet air deflection aided by compressed air gas. At the end of the deposition of nanomaterials, fabrics were dried on a heat plate at 50°C for 1 day.

By using an ultrasonic spraying technique, four distinct dispersions were deposited on glass fiber surfaces: ox-SWCNTs, SEPPS-SWCNT dispersions with 1:1 and 2:1 weight ratios, and SEPPS alone. In all spray deposition experiments, 10, 20 and 30 mg/m<sup>2</sup> deposition of SWCNTs were aimed on each surface of glass fiber fabrics by controlling the total amount of dispersion sprayed onto each unit surface. In the case SEPPS, the same depositions amounts were aimed by weight of SEPPS.

#### **4.4. Composite production by Vacuum Infusion Method**

Vacuum infusion process was used to fabricate FRPC plates from the prepared fabrics. Additionally, a reference plate without any SWCNT or SEPPS incorporation was produced. The table was cleaned with a cleaner prior to the production. Following the cleaning, four layers of a sealer were applied at 15-minute intervals to conceal the table's defects. Following the application of four layers of sealer, four layers of a releaser were applied at 15-minute intervals again. After the preparation of the table, glass fiber fabrics were lined up layer by layer in the desired plate size. A flow mesh was used to wet the glass fiber fabrics uniformly and the peel ply is used to prevent the plies from adhering to the flow mesh. In addition, perforated Teflon sheet was also placed in between the peel ply and flow mesh to slow down the resin flow and provide a better wetting. Then, a vacuum bag was used to enclose the glass layers over the production area, and lastly, sealing tape was used around the edges to keep the whole system in the vacuum. (Figure 32). To prevent sanding the samples after manufacturing, a peel ply was also put between the table and the plates while producing tensile test samples.

Prior to vacuum infusion, after mixing the epoxy resin and hardener, a half-hour of degassing was conducted. Meanwhile, air inside the vacuum bag was evacuated, the pressure inside was lowered to zero, and the vacuum bag was checked for air leak. The degassed resin was then vacuum infused. The plates were cured for three days at atmospheric pressure and ambient temperature, and then post-cured for one day at 70°C. The plates were removed from the table after four days. Composite plate produced by vacuum infusion process was shown on Figure 33.

Four different experimental groups were prepared throughout the experiment. In each production, one more plate was produced without any nanoparticle deposition as a reference. For all experimental groups, the nanoparticles were SWCNT, dispersion medium was water, concentration of dispersions was 0.05 wt%, drying procedure of the fabrics was 50°C, reinforcer was GF and epoxy resin was Biresin CR80. Experimental groups and samples are shown in Table 1.

Table 1 Four different composite plates including SEPPS and SWCNT deposited with variable parameters

Sample Name	Silane	Silane/NP	mg/m <sup>2</sup> (each side)
Reference	-	-	-
Ox-CNT 10 mg/m <sup>2</sup>	-	-	10
Ox-CNT 20 mg/m <sup>2</sup>	-	-	20
Ox-CNT 30 mg/m <sup>2</sup>	-	-	30
SEPPS 10 mg/m <sup>2</sup>	SEPPS	-	10
SEPPS 20 mg/m <sup>2</sup>	SEPPS	-	20
SEPPS 30 mg/m <sup>2</sup>	SEPPS	-	30
SEPPS-CNT (1:1) 10 mg/m <sup>2</sup>	SEPPS	1	10
SEPPS-CNT (1:1) 20 mg/m <sup>2</sup>	SEPPS	1	20
SEPPS-CNT (1:1) 30 mg/m <sup>2</sup>	SEPPS	1	30
SEPPS-CNT (2:1) 10 mg/m <sup>2</sup>	SEPPS	2	10
SEPPS-CNT (2:1) 20 mg/m <sup>2</sup>	SEPPS	2	20
SEPPS-CNT (2:1) 30 mg/m <sup>2</sup>	SEPPS	2	30



Figure 32 Steps of vacuum infusion process

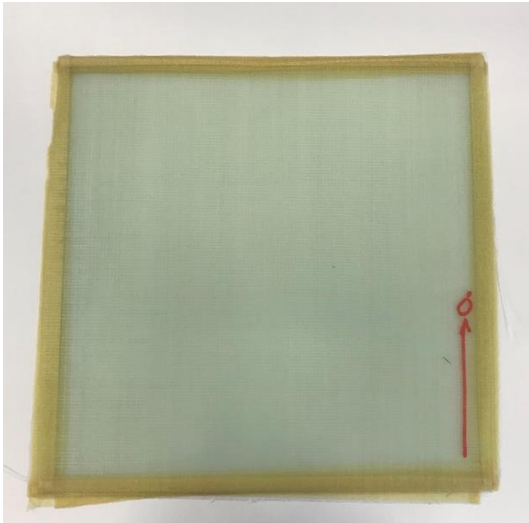


Figure 33 Produced composite plate after vacuum infusion process.

#### 4.5. Sample preparation for mechanical, thermal and structural characterizations

The produced FRPC plates were trimmed with water jet, then the tensile test specimens were cut according to ASTM D 3039 standard, again using the water jet. A wet diamond cutter was used to produce TGA, DMA, DSC, and pycnometer samples.

Tensile test specimens were cut from the produced plate in the 0° direction. As stated in ASTM standards, the sample was 250 mm in length and 25 mm in width. Additionally, they were tabbed using two component Araldite® 2011 adhesive on both sides with a span length of 150 mm, using tabs measured 50 mm in length and 25 mm in width (see

Figure 34).

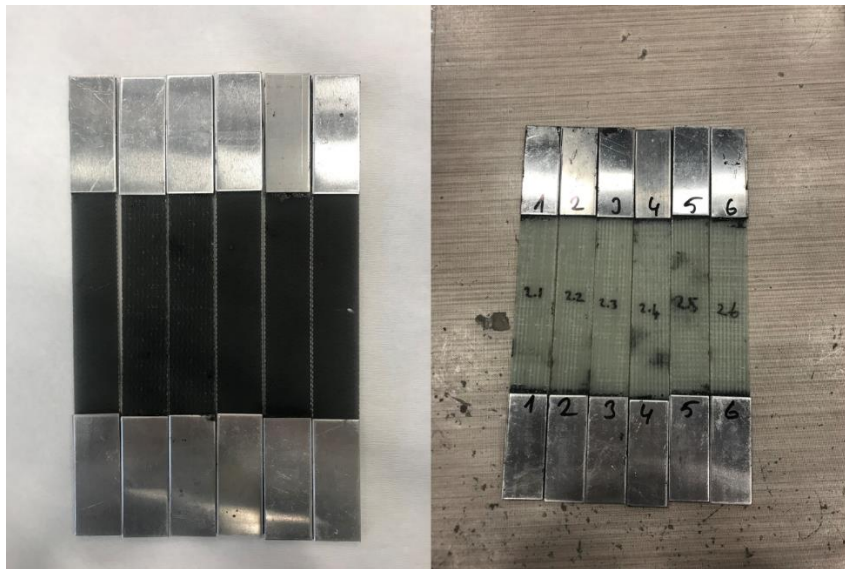


Figure 34 Tensile test specimens of CNT reinforced GF composite (*left*), neat GF composite (*right*)

For each FRPC sample, a minimum of 6 specimens were tested using INSTRON 5982 100 kN Universal Testing Systems, and the results were analyzed using Blue hill® software. At a rate of 2mm/min, the axial load was applied. As seen in Figure 35, for the examination of precise strain data, a biaxial clip-on extensometer was fixed on the specimen and connected to the testing equipment. One of the tensile test specimens before and after the tensile test was shown in Figure 36.



Figure 35 Tensile test setup



Figure 36 Tensile test specimen before (left) and after (right) tensile test

Selected FRPCs were subjected to dynamic mechanical analysis (DMA) using a Mettler Toledo DMA instrument. The dynamic storage modulus and tan delta values were obtained as a result of experiments conducted at a frequency of 1Hz from 25°C to 200°C with a 3 K/min increase in temperature.

## 4.6. Results and Discussion

### 4.6.1. Structural characterization of FRPCs

The resin, fiber, and void ratios and densities of the produced plates were determined by the density of composite (ASTM D792) and void content of the composite (ASTM D2734) analysis. We were able to determine the void content of each composite structure using the fiber-resin content and density of each plate, as presented in Table 2. The resin and void content of each plate was found to be consistent in plates to be mechanically tested.

Table 2 Properties of manufactured composites, average density, void content, fiber-resin

Sample Name	Average Density (g/cm <sup>3</sup> )	Void Content (volume%)	Fiber wt%	Resin wt%
Reference	1,76	0,87	60,64	39,36
Ox-CNT 10 mg/m <sup>2</sup>	1,81	0,51	65,44	34,56
Ox-CNT 20 mg/m <sup>2</sup>	1,78	1,28	64,89	35,11
Ox-CNT 30 mg/m <sup>2</sup>	1,76	1,76	64,21	35,79
SEPPS 10 mg/m <sup>2</sup>	1,79	0,97	65,07	34,93
SEPPS 20 mg/m <sup>2</sup>	1,79	0,05	63,91	36,09
SEPPS 30 mg/m <sup>2</sup>	1,80	0,21	64,45	35,55
SEPPS-CNT (1:1) 10 mg/m <sup>2</sup>	1,79	1,57	65,89	34,11
SEPPS-CNT (1:1) 20 mg/m <sup>2</sup>	1,80	0,69	65,45	34,55
SEPPS-CNT (1:1) 30 mg/m <sup>2</sup>	1,80	0,68	63,93	36,07
SEPPS-CNT (2:1) 10 mg/m <sup>2</sup>	1,78	0,72	62,43	37,57
SEPPS-CNT (2:1) 20 mg/m <sup>2</sup>	1,79	0,76	62,67	37,33
SEPPS-CNT (2:1) 30 mg/m <sup>2</sup>	1,77	0,64	61,96	38,04

#### 4.6.2. Mechanical characterization of FRPCs

##### 4.6.2.1. Tensile tests

As summarized in Table 3, tensile tests of fabricated FRPCs revealed that both Young's modulus and tensile strength values increased when compared to the reference sample in all FRPC samples containing ox-SWCNTs, SEPPS or different ratios of SEPPS and SWCNTs. In the first group, when 10 mg of ox-CNT was sprayed per square meter of glass fiber fabric, the Young's modulus increased to approximately 23 GPa as the most significant improvement in this group of FRPCs samples with an approximately 19% increase (Figure 39). In the case of tensile strength, as in Figure 40 the incorporation of 20 mg of ox-CNT per square meter resulted in a tensile strength value of 475 MPa, which represents a 55% increase above the reference.

In the second group of samples, in which SEPPS alone was incorporated, Young's modulus (see Table 3) values increased in all three different spray deposition amounts, as in the first group. The highest improvement was seen in the FRPC sample with 30 mg of SEPPS per square meter at a strength of almost 22 GPa. 13.70% increase was observed in the Young's Modulus of this set of samples compared to the reference as shown in Figure 39. Additionally, the change in the Young's modulus was directly proportional to the amount of SEPPS sprayed on the surface in this group. When the tensile strength values were compared to the reference, all three SEPPS-containing samples had greater values (Figure 37 top right). In this case, 10 mg SEPPS per square meter reached the highest tensile strength value in this group with approximately 465 MPa, providing an increase of 51% compared to the reference.

When FRPC plates were reinforced with SWCNTs in the presence of SEPPS at a 1:1 ratio by weight, all samples in this group resulted in an increase in Young's modulus and tensile strength values when compared to the reference sample. The sample prepared with 30 mg per square meter resulted in the highest Young's modulus, as shown in the Table 3. In addition, both the Young's modulus and tensile strength proportionately increased with the increasing amount of spray-deposited SEPPS-SWCNT. As shown in Figure 40 and Figure 37 bottom left, 30 mg of SWCNTs with 30 mg of SEPPS sprayed per square meter increased the tensile strength of the reference plate by 47% with approximately 451 MPa.

When the amount of SEPPS was double compared to that of CNT in the aqueous dispersion prepared for the spray deposition, a less significant improvement was observed in Young's modulus values. The composite plate with 30 mg SWCNTs per square meter showed the greatest increase in this group, by 8.45 %. The improvement in the tensile strength values was more significant, the samples with 30 mg/m<sup>2</sup> spray deposited SWCNTs had a tensile strength value of 487 MPa, an increase of about 59% above the reference plate. Yet, there was not a linear relationship between neither Young's modulus nor tensile strength and SWCNT deposition amount in this group of samples.

Table 3 Tensile test results of FRPCs produced with VIP

Sample Name	Young's Modulus, GPa	Tensile Strain, (%)	Tensile Strength, MPa
Reference	19,31±0,31	2,76±0,16	307,34±12,36
Ox-CNT 10 mg/m <sup>2</sup>	22,94±1,68	3,71±0,28	440,76±30,61
Ox-CNT 20 mg/m <sup>2</sup>	21,78±0,51	4,58±0,50	475,42±44,88
Ox-CNT 30 mg/m <sup>2</sup>	22,25±1,22	4,38±0,32	462,47±29,07
SEPPS 10 mg/m <sup>2</sup>	21,18±0,52	4,27±0,35	465,31±23,37
SEPPS 20 mg/m <sup>2</sup>	21,58±0,50	3,46±0,26	376,19±15,33
SEPPS 30 mg/m <sup>2</sup>	21,95±0,91	4,03±0,29	425,32±17,35
SEPPS-CNT (1:1) 10 mg/m <sup>2</sup>	20,81±0,58	2,54±0,18	317,81±17,60
SEPPS-CNT (1:1) 20 mg/m <sup>2</sup>	21,74±0,82	3,64±0,17	423,13±9,80
SEPPS-CNT (1:1) 30 mg/m <sup>2</sup>	22,27±0,63	4,00±0,15	451,76±10,67
SEPPS-CNT (2:1) 10 mg/m <sup>2</sup>	20,24±0,33	4,17±0,12	476,86±11,92
SEPPS-CNT (2:1) 20 mg/m <sup>2</sup>	20,57±0,72	3,82±0,19	451,53±21,17
SEPPS-CNT (2:1) 30 mg/m <sup>2</sup>	20,94±0,60	4,09±0,28	487,94±30,86

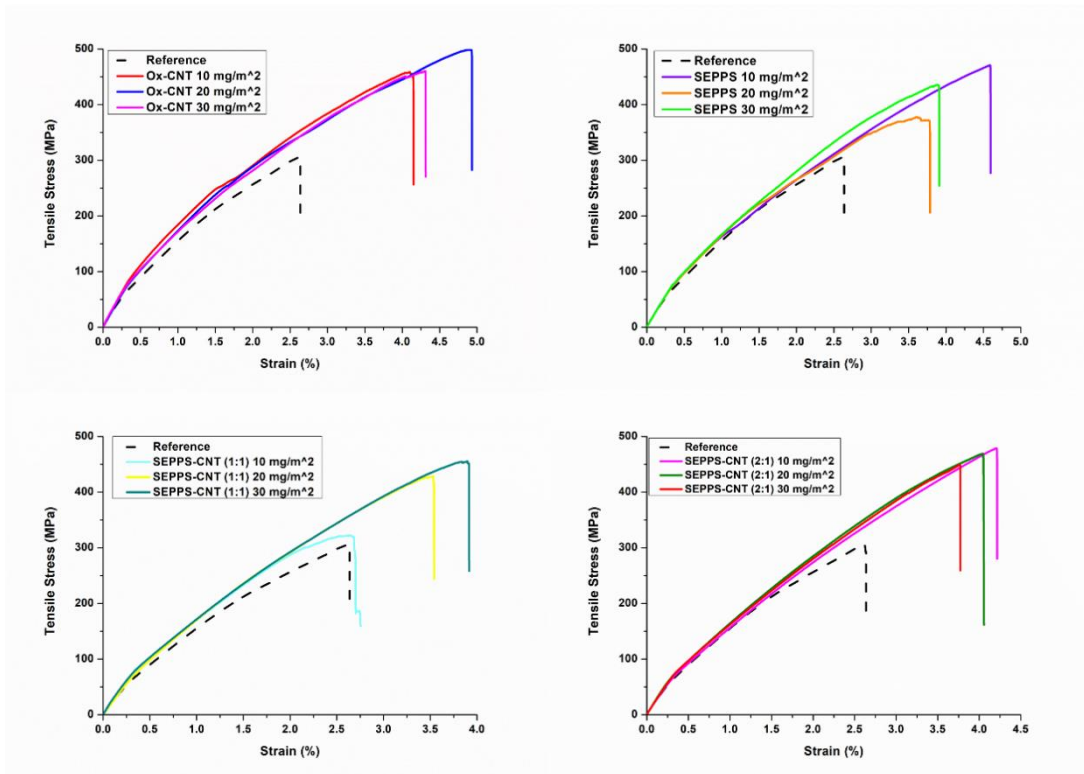


Figure 37 Tensile test results of Ox-SWCNT reinforced (top left), SEPPS reinforced (top right), SEPPS-SWCNT (2:1) reinforced (bottom left) and SEPPS-SWCNT (1:1) reinforced (bottom right) FRPC samples

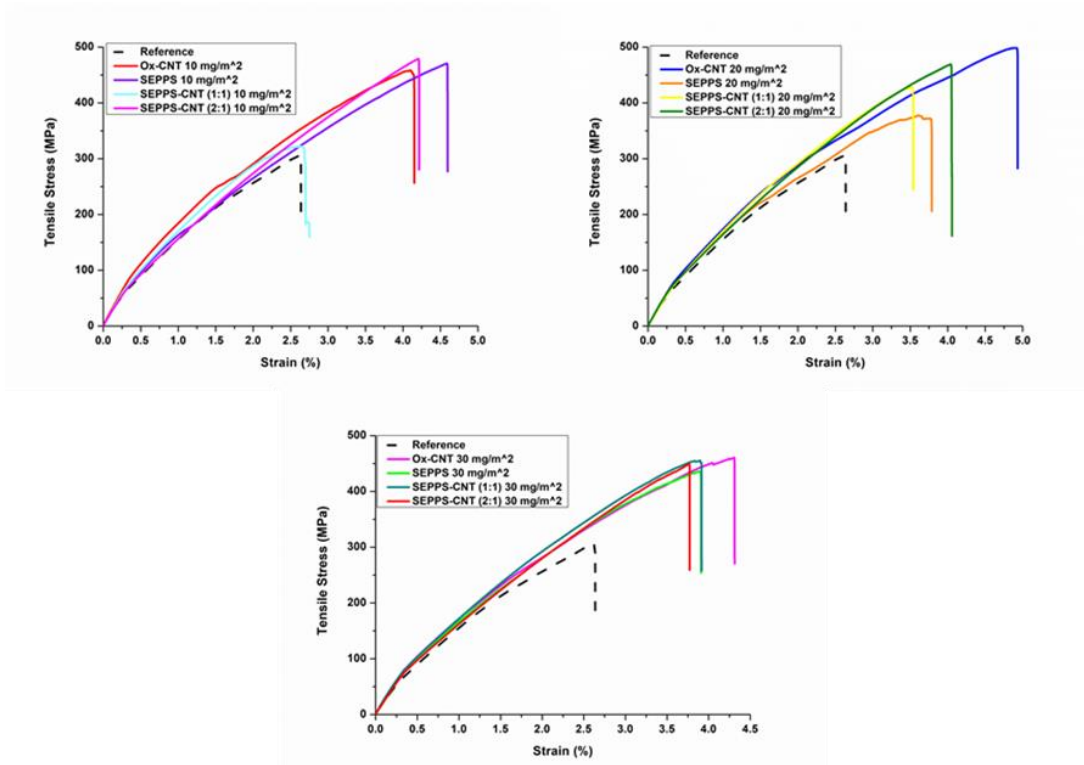


Figure 38 Tensile test results of FRPC samples containing 10 mg/m<sup>2</sup> (top left) 20mg/m<sup>2</sup> (top right) and, 30 mg/m<sup>2</sup> (bottom) carbon nanomaterials in comparison with reference and only SEPPS containing samples

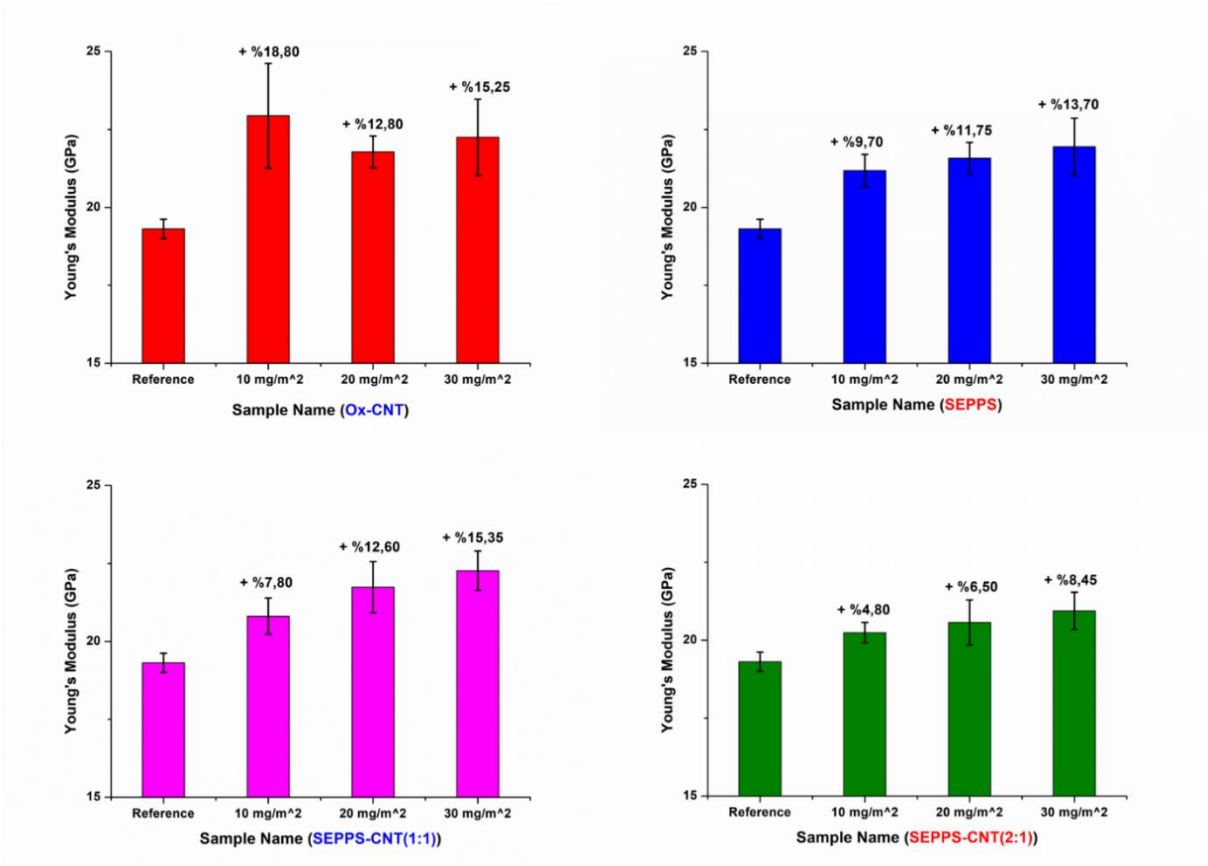


Figure 39 Changes in the Young's Modulus values of FRPC samples containing Ox-SWCNTs, SEPPS or SEPPS-SWCNT mixtures in comparison with the reference

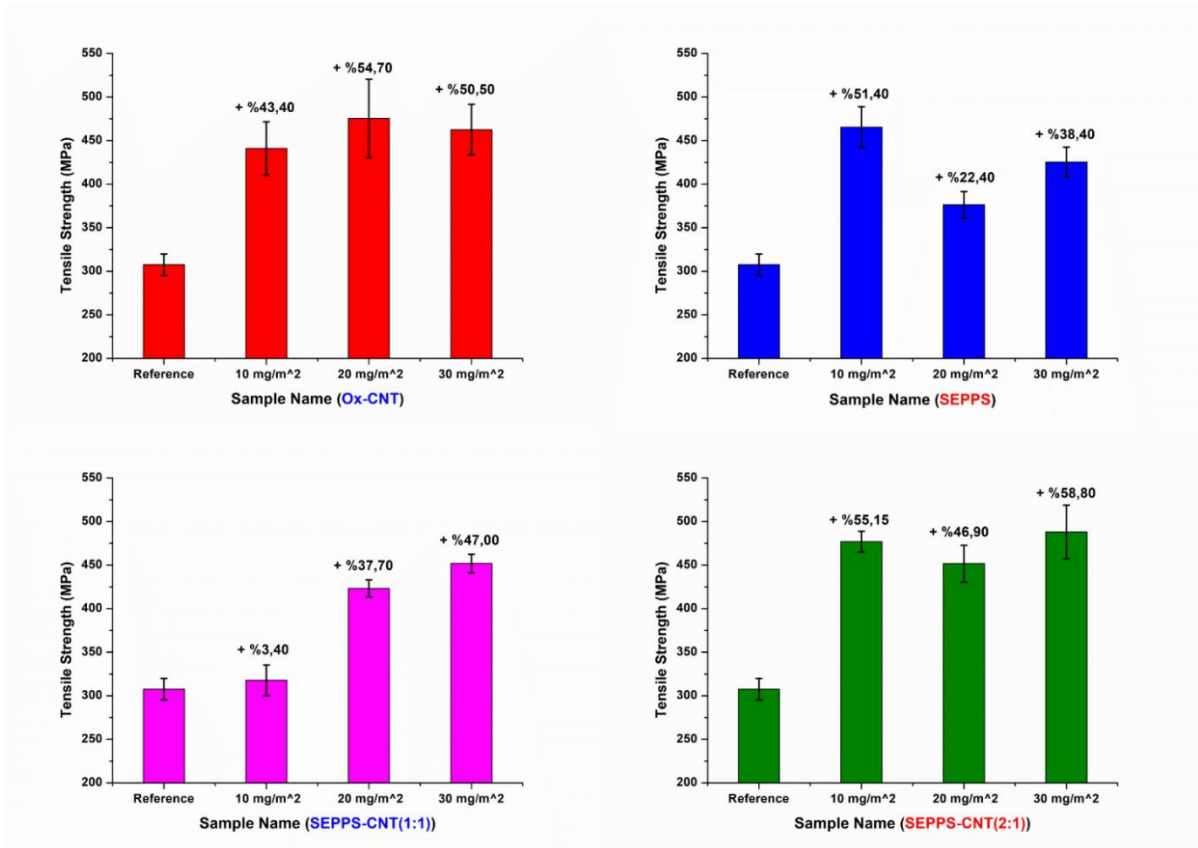


Figure 40 Changes in the tensile strength values of FRPC samples containing Ox-SWCNTs, SEPPS or SEPPS-SWCNT mixtures in comparison with the reference

### 4.6.3. Thermo-mechanical Analysis of FRPCs

#### 4.6.3.1. Dynamic Mechanical Analysis (DMA)

The dynamic storage modulus ( $E'$ ) is an important property that can be determined by measuring the energy stored owing to the elastic behaviour of a material. As shown in Figure 41, it was found that the  $E'$  value of FRPC samples decreased significantly with increasing temperature in both the reference and nanomaterial reinforced plates, particularly between 80°C and 85°C, where the glass transition ( $T_g$ ) occurs. This reduction is explained by the material's phase transition from a glassy to a rubbery state because of an increase in the mobility of the molecular chains as the temperature increases. Due to the decreased interfacial interactions between the matrix and the fibers after  $T_g$ , the material's resistance to elongation, or stiffness, diminished.

There was no significant reduction in the  $T_g$  values of the selected samples in this study (see Figure 42). When the dynamic storage modulus is compared before the glass transition, composite samples reinforced with SEPPS-SWCNT had higher  $E'$  values than the reference. The increase in storage modulus in relation to the Young's modulus values in tensile test results

further demonstrated that reinforced composites had enhanced mechanical and thermomechanical characteristics.

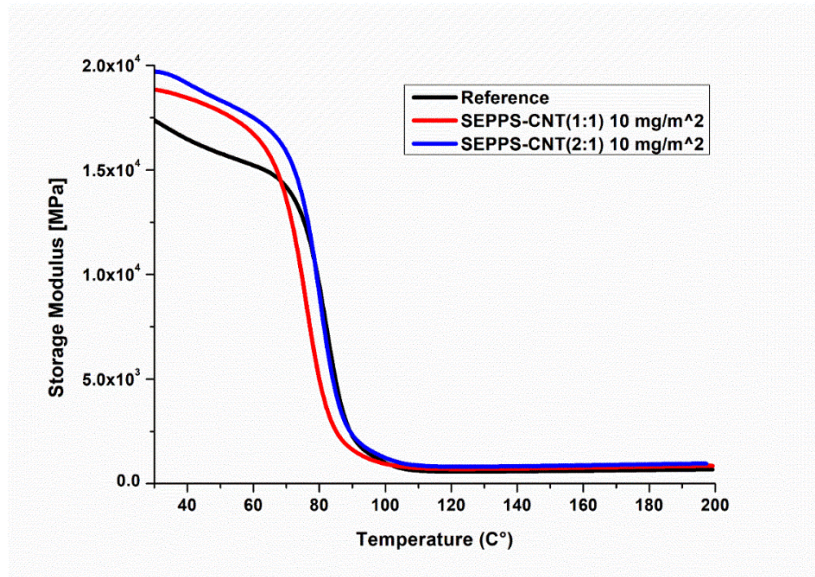


Figure 41 Storage modulus of reference and selected nano-reinforced FRPC samples

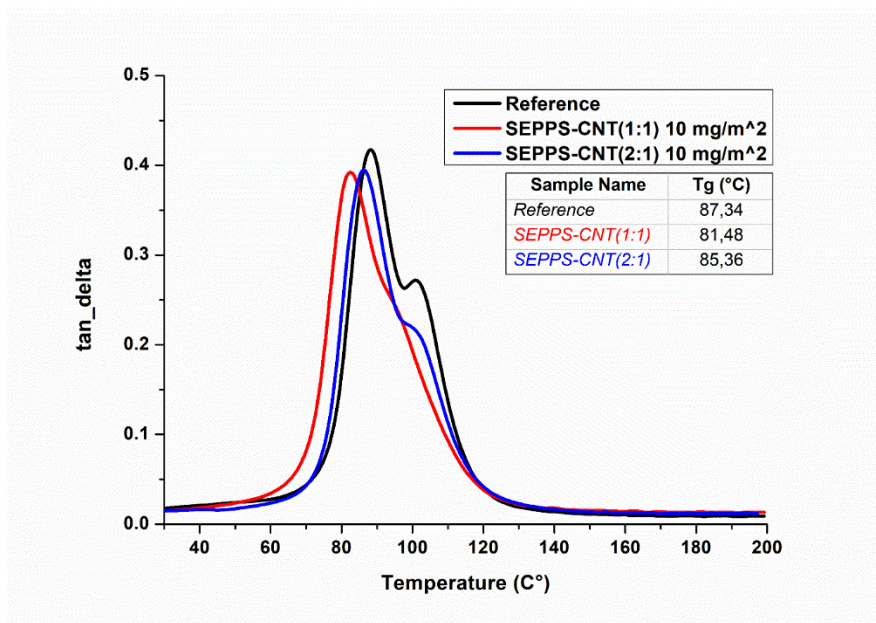


Figure 42 Tan delta results of reference and selected nano-reinforced FRPC samples

#### 4.6.4. Thermal Characterization of FRPCs

##### 4.6.4.1. Differential Scanning Calorimetry (DSC)

The thermal characterizations of manufactured composite samples were carried out to assess any issues related with the curing efficiency and changes in the  $T_g$  of samples containing SEPPS and SWCNTs in comparison to a reference sample. When the DSC data were compared to the reference, SEPPS-SWCNT containing samples'  $T_g$  values was slightly lower than the reference

samples, yet they were all in an acceptable range above 80 °C. The fact that the  $T_g$  values of the produced plates did not vary significantly from the reference indicated that the sprayed SEPPS with SWCNTs had no negative impact on the curing behaviour of the resin and the final composites' thermal characteristics. Additionally, the fact that the DSC and tan delta findings from the DMA analyses were consistent demonstrated the reliability. Slight decreases in  $T_g$  of plates containing nanomaterials are shown in Figure 43

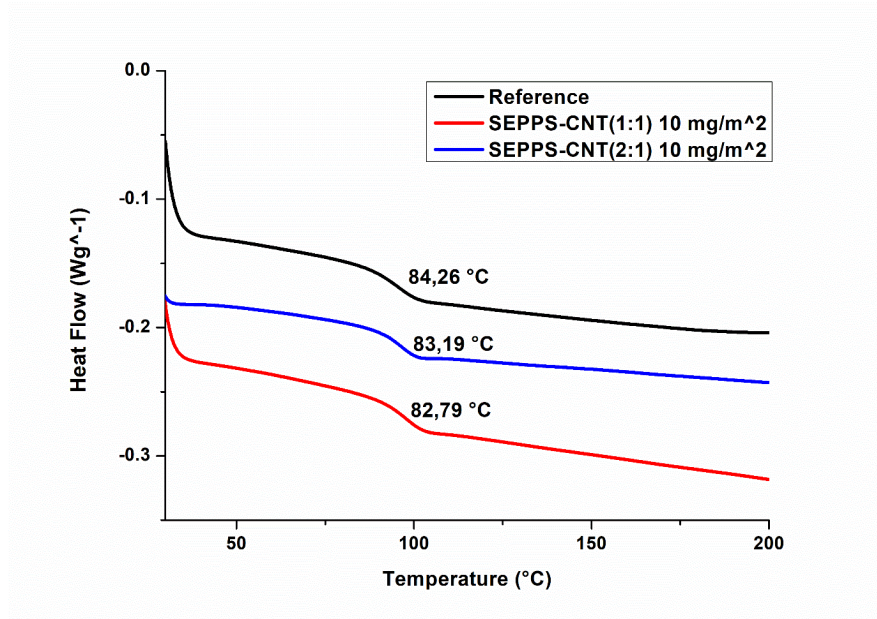


Figure 43 DSC thermograms of reference and selected nano-reinforced FRPC samples

#### 4.7. Conclusions

Oxidized SWCNTs were dispersed in water in the presence of a multi-functional silane compound, SEPPS, and uniformly deposited on glass fiber fabrics by using an ultrasonic spraying technique. Then, utilizing these fibers, vacuum infusion process was used to produce various SWCNT reinforced FRPCs. Fiber to resin ratio determination, void content and density measurements were performed to verify that the manufactured plates were comparable. The plates were found to be appropriate for thermal, thermomechanical, and mechanical testing and in accordance with the standards required for these tests. Significant improvements were observed in the mechanical behaviour of FRPC samples containing SWCNTs and/or SEPPS. In fact, even the incorporation of SEPPS compound alone resulted in significant improvements in the mechanical properties of FRPCs, demonstrating that the designed, multi-functional silane compound, SEPPS alone was able to significantly contribute to load transfer at the matrix-fiber

interface. The incorporation of SWCNTs in the presence of SEPPS was demonstrated to improve the mechanical properties, tensile strength and Young's modulus of resulting FRPCs more systematically, as a function of the SWCNT content especially when a 1:1 ratio of SEPPS to SWCNTs was used in the dispersion. DMA results demonstrated that the incorporation of SEPPS and SWCNTs at the fiber-polymer interface improved the storage modulus of resulting FRPCs below the glass transition. Additionally, the examination of  $T_g$  values from DMA and DSC analysis demonstrated that the incorporation of SEPPS and/or SWCNTs into the interface had no negative impact on the epoxy matrix's curing behavior.

## References

- [1] M. S. S. Prasad, C. S. Venkatesha, and T. Jayaraju, "Experimental Methods of Determining Fracture Toughness of Fiber Reinforced Polymer Composites under Various Loading Conditions," *Journal of Minerals and Materials Characterization and Engineering*, vol. 10, no. 13, pp. 1263–1275, 2011, doi: 10.4236/jmmce.2011.1013099.
- [2] J. M. Wernik and S. A. Meguid, "Recent developments in multifunctional nanocomposites using carbon nanotubes," *Applied Mechanics Reviews*, vol. 63, no. 5, pp. 1–40, 2010, doi: 10.1115/1.4003503.
- [3] P. M. Ajayan, O. Stephan, C. Colliex, and D. Trauth, "Aligned Carbon Nanotube Arrays Formed by Cutting a Polymer Resin Aligned Carbon Nanotube Arrays Formed by Cutting a Polymer Resin Nanotube Composite Aligned Carbon Nanotube Arrays Formed by Cutting a Polymer Resin N ...," *Carbon letters*, vol. 265, no. August, pp. 1212–1214, 2006.
- [4] M. Theodore, M. Hosur, J. Thomas, and S. Jeelani, "Influence of functionalization on properties of MWCNT-epoxy nanocomposites," *Materials Science and Engineering A*, vol. 528, no. 3, pp. 1192–1200, 2011, doi: 10.1016/j.msea.2010.09.095.
- [5] S. J. V. Frankland, A. Caglar, D. W. Brenner, and M. Griebel, "Molecular simulation of the influence of chemical cross-links on the shear strength of carbon nanotube-polymer interfaces," *Journal of Physical Chemistry B*, vol. 106, no. 12, pp. 3046–3048, 2002, doi: 10.1021/jp015591+.
- [6] J. Zhang, R. Zhuang, J. Liu, E. Mäder, G. Heinrich, and S. Gao, "Functional interphases with multi-walled carbon nanotubes in glass fibre/epoxy composites," *Carbon*, vol. 48, no. 8, pp. 2273–2281, 2010, doi: 10.1016/j.carbon.2010.03.001.
- [7] P. C. Ma, J. K. Kim, and B. Z. Tang, "Functionalization of carbon nanotubes using a silane coupling agent," *Carbon*, vol. 44, no. 15, pp. 3232–3238, 2006, doi: 10.1016/j.carbon.2006.06.032.
- [8] Michael F. L.; De Volder, Sameh H.; Tawfick, Ray H.; Baughman, and A. John ;Hart, "Carbon Nanotubes: Present and Future Commercial Applications," *Science*, vol. 339, no. 6119, pp. 535–539, 2013, [Online]. Available: <http://science.sciencemag.org/content/339/6119/535?sid=599bece0-48b5-4fcc-9d21-5e29be89422c>
- [9] E. P. Koumoulos *et al.*, "Research and Development in Carbon Fibers and Advanced High-Performance Composites Supply Chain in Europe: A Roadmap for Challenges and the Industrial Uptake," *Journal of Composites Science*, vol. 3, no. 3, p. 86, 2019, doi: 10.3390/jcs3030086.
- [10] K. A. Wepasnick, B. A. Smith, K. E. Schrote, H. K. Wilson, S. R. Diegelmann, and D. H. Fairbrother, "Surface and structural characterization of multi-walled carbon nanotubes following different oxidative treatments," *Carbon*, vol. 49, no. 1, pp. 24–36, 2011, doi: 10.1016/j.carbon.2010.08.034.
- [11] W. Yu, L. Sisi, Y. Haiyan, and L. Jie, "Progress in the functional modification of graphene/graphene oxide: A review," *RSC Advances*, vol. 10, no. 26, pp. 15328–15345, 2020, doi: 10.1039/d0ra01068e.

- [12] G. Gong, "Literature study of graphene modified polymeric composites," p. 57, 2018, [Online]. Available: <https://siografen.se/app/uploads/2018/02/Literature-study-of-Graphene-modified-polymeric-composites.pdf>
- [13] W. L. Zhang, B. J. Park, and H. J. Choi, "Colloidal graphene oxide/polyaniline nanocomposite and its electrorheology," *Chemical Communications*, vol. 46, no. 30, pp. 5596–5598, 2010, doi: 10.1039/c0cc00557f.
- [14] J. K. Lee, S. Song, and B. Kim, "Functionalized graphene sheets-epoxy based nanocomposite for cryotank composite application," *Polymer Composites*, vol. 33, no. 8, pp. 1263–1273, 2012, doi: 10.1002/pc.22251.
- [15] M. J. Mcallister *et al.*, "Expansion of Graphite," *Society*, vol. 19, no. 4, pp. 4396–4404, 2007, doi: 10.1021/cm0630800.
- [16] H. C. Schniepp *et al.*, "Functionalized single graphene sheets derived from splitting graphite oxide," *Journal of Physical Chemistry B*, vol. 110, no. 17, pp. 8535–8539, 2006, doi: 10.1021/jp060936f.
- [17] X. Zhang *et al.*, "Interfacial microstructure and properties of carbon fiber composites modified with graphene oxide," *ACS Applied Materials and Interfaces*, vol. 4, no. 3, pp. 1543–1552, 2012, doi: 10.1021/am201757v.
- [18] A. K. Geim and K. S. Novoselov, "The rise of graphene PROGRESS," *Nature Materials*, vol. 6, no. 3, pp. 183–191, 2007.
- [19] C. Probig, R. F. Curl, and R. E. Smalley, "O<sub>i</sub>G 44," 1985.
- [20] W. Krätschmer, L. D. Lamb, K. Fostiropoulos, and D. R. Huffman, "Solid C<sub>60</sub>: a new form of carbon," *Nature*, vol. 347, no. 6291, pp. 354–358, 1990, doi: 10.1038/347354a0.
- [21] J. Ortiz Balbuena, P. Tutor De Ureta, E. Rivera Ruiz, and S. Mellor Pita, "Enfermedad de Vogt-Koyanagi-Harada," *Medicina Clinica*, vol. 146, no. 2, pp. 93–94, 2016, doi: 10.1016/j.medcli.2015.04.005.
- [22] Y. Zhang, Y. W. Tan, H. L. Stormer, and P. Kim, "Experimental observation of the quantum Hall effect and Berry's phase in graphene," *Nature*, vol. 438, no. 7065, pp. 201–204, 2005, doi: 10.1038/nature04235.
- [23] K. S. Novoselov *et al.*, "Room-Temperature Quantum Hall," vol. 315, no. March, p. 2007, 2007.
- [24] K. S. Novoselov *et al.*, "Two-dimensional gas of massless Dirac fermions in graphene," *Nature*, vol. 438, no. 7065, pp. 197–200, 2005, doi: 10.1038/nature04233.
- [25] K. Wang, M. Xu, Y. Gu, Z. Gu, J. Liu, and Q. H. Fan, "Low-temperature plasma exfoliated n-doped graphene for symmetrical electrode supercapacitors," *Nano Energy*, vol. 31, no. December 2016, pp. 486–494, 2017, doi: 10.1016/j.nanoen.2016.11.007.
- [26] V. Singh, D. Joung, L. Zhai, S. Das, S. I. Khondaker, and S. Seal, "Graphene based materials: Past, present and future," *Progress in Materials Science*, vol. 56, no. 8, pp. 1178–1271, 2011, doi: 10.1016/j.pmatsci.2011.03.003.
- [27] D. R. Dreyer, A. D. Todd, and C. W. Bielawski, "Harnessing the chemistry of graphene oxide," *Chemical Society Reviews*, vol. 43, no. 15, pp. 5288–5301, 2014, doi: 10.1039/c4cs00060a.

- [28] S. Stankovich *et al.*, "Synthesis of graphene-based nanosheets via chemical reduction of exfoliated graphite oxide," *Carbon*, vol. 45, no. 7, pp. 1558–1565, 2007, doi: 10.1016/j.carbon.2007.02.034.
- [29] D. Tasis, N. Tagmatarchis, A. Bianco, and M. Prato, "Chemistry of carbon nanotubes," *Chemical Reviews*, vol. 106, no. 3, pp. 1105–1136, 2006, doi: 10.1021/cr050569o.
- [30] P. M. Ajayan, "Nanotubes from Carbon," *Chemical Reviews*, vol. 99, no. 7, pp. 1787–1799, 1999, doi: 10.1021/cr970102g.
- [31] H. Dai, "Carbon nanotubes: Synthesis, integration, and properties," *Accounts of Chemical Research*, vol. 35, no. 12, pp. 1035–1044, 2002, doi: 10.1021/ar010164o.
- [32] E. W. Wong, P. E. Sheehan, and C. M. Lieber, "Nanobeam mechanics: Elasticity, strength, and toughness of nanorods and nanotubes," *Science*, vol. 277, no. 5334, pp. 1971–1975, 1997, doi: 10.1126/science.277.5334.1971.
- [33] O. Lourie and H. D. Wagner, "Evaluation of Young's modulus of carbon nanotubes by micro-Raman spectroscopy," *Journal of Materials Research*, vol. 13, no. 9, pp. 2418–2422, 1998, doi: 10.1557/JMR.1998.0336.
- [34] M. F. Yu, O. Lourie, M. J. Dyer, K. Moloni, T. F. Kelly, and R. S. Ruoff, "Strength and breaking mechanism of multiwalled carbon nanotubes under tensile load," *Science*, vol. 287, no. 5453, pp. 637–640, 2000, doi: 10.1126/science.287.5453.637.
- [35] J. N. Coleman, U. Khan, W. J. Blau, and Y. K. Gun'ko, "Small but strong: A review of the mechanical properties of carbon nanotube-polymer composites," *Carbon*, vol. 44, no. 9, pp. 1624–1652, 2006, doi: 10.1016/j.carbon.2006.02.038.
- [36] Z. Kordrostami, M. H. Sheikhi, and R. Mohammadzadegan, "Modeling electronic properties of multiwall carbon nanotubes," *Fullerenes Nanotubes and Carbon Nanostructures*, vol. 16, no. 1, pp. 66–77, 2008, doi: 10.1080/15363830701783713.
- [37] P. L. McEuen, M. S. Fuhrer, and H. Park, "Single-walled carbon nanotube electronics," *IEEE Transactions on Nanotechnology*, vol. 1, no. 1, pp. 78–84, 2002, doi: 10.1109/TNANO.2002.1005429.
- [38] B. Q. Wei, R. Vajtai, and P. M. Ajayan, "Reliability and current carrying capacity of carbon nanotubes," *Applied Physics Letters*, vol. 79, no. 8, pp. 1172–1174, 2001, doi: 10.1063/1.1396632.
- [39] Z. Zhao *et al.*, "Mechanical, thermal and interfacial performances of carbon fiber reinforced composites flavored by carbon nanotube in matrix/interface," *Composite Structures*, vol. 159, pp. 761–772, 2017, doi: 10.1016/j.compstruct.2016.10.022.
- [40] P. C. Ma, S. Y. Mo, B. Z. Tang, and J. K. Kim, "Dispersion, interfacial interaction and re-agglomeration of functionalized carbon nanotubes in epoxy composites," *Carbon*, vol. 48, no. 6, pp. 1824–1834, 2010, doi: 10.1016/j.carbon.2010.01.028.
- [41] H. Qian, E. S. Greenhalgh, M. S. P. Shaffer, and A. Bismarck, "Carbon nanotube-based hierarchical composites: A review," *Journal of Materials Chemistry*, vol. 20, no. 23, pp. 4751–4762, 2010, doi: 10.1039/c000041h.

- [42] R. Sadeghian, S. Gangireddy, B. Minaie, and K. T. Hsiao, "Manufacturing carbon nanofibers toughened polyester/glass fiber composites using vacuum assisted resin transfer molding for enhancing the mode-I delamination resistance," *Composites Part A: Applied Science and Manufacturing*, vol. 37, no. 10, pp. 1787–1795, 2006, doi: 10.1016/j.compositesa.2005.09.010.
- [43] A. J. Rodriguez, M. E. Guzman, C. S. Lim, and B. Minaie, "Mechanical properties of carbon nanofiber/fiber-reinforced hierarchical polymer composites manufactured with multiscale-reinforcement fabrics," *Carbon*, vol. 49, no. 3, pp. 937–948, 2011, doi: 10.1016/j.carbon.2010.10.057.
- [44] E. T. Thostenson, W. Z. Li, D. Z. Wang, Z. F. Ren, and T. W. Chou, "Carbon nanotube/carbon fiber hybrid multiscale composites," *Journal of Applied Physics*, vol. 91, no. 9, pp. 6034–6037, 2002, doi: 10.1063/1.1466880.
- [45] E. J. Garcia, B. L. Wardle, and A. J. Hart, "Composites : Part A Joining prepreg composite interfaces with aligned carbon nanotubes," vol. 39, pp. 1065–1070, 2008, doi: 10.1016/j.compositesa.2008.03.011.
- [46] E. Bekyarova *et al.*, "Multiscale carbon nanotube-carbon fiber reinforcement for advanced epoxy composites," *Langmuir*, vol. 23, no. 7, pp. 3970–3974, 2007, doi: 10.1021/la062743p.
- [47] R. J. Sager *et al.*, "Effect of carbon nanotubes on the interfacial shear strength of T650 carbon fiber in an epoxy matrix," *Composites Science and Technology*, vol. 69, no. 7–8, pp. 898–904, 2009, doi: 10.1016/j.compscitech.2008.12.021.
- [48] S. C. Patel, O. Alam, D. Zhang, K. Grover, Y. X. Qin, and B. Sitharaman, "Layer-by-layer, ultrasonic spray assembled 2D and 3D chemically crosslinked carbon nanotubes and graphene," *Journal of Materials Research*, vol. 32, no. 2, pp. 370–382, 2017, doi: 10.1557/jmr.2016.472.
- [49] Z. Wu *et al.*, "Transparent, conductive carbon nanotube films," *Science*, vol. 305, no. 5688, pp. 1273–1276, 2004, doi: 10.1126/science.1101243.
- [50] R. C. Tenent *et al.*, "Ultrasoother, large-area, high-uniformity, conductive transparent single-walled-carbon-nanotube films for photovoltaics produced by ultrasonic spraying," *Advanced Materials*, vol. 21, no. 31, pp. 3210–3216, 2009, doi: 10.1002/adma.200803551.
- [51] J. G. Tait *et al.*, "Spray coated high-conductivity PEDOT:PSS transparent electrodes for stretchable and mechanically-robust organic solar cells," *Solar Energy Materials and Solar Cells*, vol. 110, pp. 98–106, 2013, doi: 10.1016/j.solmat.2012.09.005.
- [52] V. H. Pham *et al.*, "Fast and simple fabrication of a large transparent chemically-converted graphene film by spray-coating," *Carbon*, vol. 48, no. 7, pp. 1945–1951, 2010, doi: 10.1016/j.carbon.2010.01.062.
- [53] K. X. Steirer *et al.*, "Ultrasonic spray deposition for production of organic solar cells," *Solar Energy Materials and Solar Cells*, vol. 93, no. 4, pp. 447–453, 2009, doi: 10.1016/j.solmat.2008.10.026.
- [54] J. Riemer, "Ultrasonic Spray Coating of Nanoparticles," *Technology*, no. February, pp. 26–28, 2011.

- [55] K. S. Sadanandan *et al.*, "Graphene coated fabrics by ultrasonic spray coating for wearable electronics and smart textiles," *JPhys Materials*, vol. 4, no. 1, 2021, doi: 10.1088/2515-7639/abc632.
- [56] T. W. Chou, L. Gao, E. T. Thostenson, Z. Zhang, and J. H. Byun, "An assessment of the science and technology of carbon nanotube-based fibers and composites," *Composites Science and Technology*, vol. 70, no. 1, pp. 1–19, 2010, doi: 10.1016/j.compscitech.2009.10.004.
- [57] A. Hirsch, "MINIREVIEW Functionalization of Single-Walled Carbon Nanotubes," no. Cvd, pp. 1853–1859, 2002.
- [58] S. W. Kim *et al.*, "Surface modifications for the effective dispersion of carbon nanotubes in solvents and polymers," *Carbon*, vol. 50, no. 1, pp. 3–33, 2011, doi: 10.1016/j.carbon.2011.08.011.
- [59] S. W. Kim *et al.*, "Surface modifications for the effective dispersion of carbon nanotubes in solvents and polymers," *Carbon*, vol. 50, no. 1, pp. 3–33, 2012, doi: 10.1016/j.carbon.2011.08.011.
- [60] Y. Xing, L. Li, C. C. Chusuei, and R. v. Hull, "Sonochemical oxidation of multiwalled carbon nanotubes," *Langmuir*, vol. 21, no. 9, pp. 4185–4190, 2005, doi: 10.1021/la047268e.
- [61] M. Monthieux, B. W. Smith, B. Burteaux, A. Claye, J. E. Fischer, and D. E. Luzzi, "Sensitivity of single-wall carbon nanotubes to chemical processing: An electron microscopy investigation," *Carbon*, vol. 39, no. 8, pp. 1251–1272, 2001, doi: 10.1016/S0008-6223(00)00249-9.
- [62] S. Banerjee, T. Hemraj-Benny, and S. S. Wong, "Covalent surface chemistry of single-walled carbon nanotubes," *Advanced Materials*, vol. 17, no. 1, pp. 17–29, 2005, doi: 10.1002/adma.200401340.
- [63] V. N. Khabashesku, W. E. Billups, and J. L. Margrave, "Fluorination of single-wall carbon nanotubes and subsequent derivatization reactions," *Accounts of Chemical Research*, vol. 35, no. 12, pp. 1087–1095, 2002, doi: 10.1021/ar020146y.
- [64] M. Holzinger *et al.*, "Sidewall functionalization of carbon nanotubes," *Angewandte Chemie - International Edition*, vol. 40, no. 21, pp. 4002–4005, 2001, doi: 10.1002/1521-3773(20011105)40:21<4002::AID-ANIE4002>3.0.CO;2-8.
- [65] R. Graupner *et al.*, "Nucleophilic-alkylation-reoxidation: A functionalization sequence for single-wall carbon nanotubes," *Journal of the American Chemical Society*, vol. 128, no. 20, pp. 6683–6689, 2006, doi: 10.1021/ja0607281.
- [66] J. Zeng, X. Kang, G. Y. Gao, F. Gao, and H. L. Zhang, "Sidewall functionalization of carbon nanotubes through electrophilic substitution," *Journal of Nanoscience and Nanotechnology*, vol. 11, no. 4, pp. 3385–3392, 2011, doi: 10.1166/jnn.2011.3750.
- [67] M. Holzinger *et al.*, "[2+1] Cycloaddition for cross-linking SWCNTs," *Carbon*, vol. 42, no. 5–6, pp. 941–947, 2004, doi: 10.1016/j.carbon.2003.12.019.
- [68] R.-O. Nitrenes *et al.*, "Functionalization of Single-Walled Carbon Nanotubes with," no. 5, pp. 8566–8580, 2003.
- [69] J. M. Tour, "Functionalization of carbon nanotubes," *AIChE Annual Meeting, Conference Proceedings*, vol. 1, p. 2403, 2004, doi: 10.1002/9783527610419.ntls0002.

- [70] C. A. Dyke and J. M. Tour, "Unbundled and highly functionalized carbon nanotubes from aqueous reactions," *Nano Letters*, vol. 3, no. 9, pp. 1215–1218, 2003, doi: 10.1021/nl034537x.
- [71] M. D. Porter, T. B. Bright, D. L. Allara, and C. E. Chidsey, "Spontaneously Organized Molecular Assemblies. 4. Structural Characterization of n-Alkyl Thiol Monolayers on Gold by Optical Ellipsometry, Infrared Spectroscopy, and Electrochemistry," *Journal of the American Chemical Society*, vol. 109, no. 12, pp. 3559–3568, 1987, doi: 10.1021/ja00246a011.
- [72] J. K. Lim *et al.*, "Selective thiolation of single-walled carbon nanotubes," *Synthetic Metals*, vol. 139, no. 2, pp. 521–527, 2003, doi: 10.1016/S0379-6779(03)00337-0.
- [73] "AN EXPERIMENTAL STUDY ON," 2014.
- [74] X. Li, Y. Qin, S. T. Picraux, and Z. X. Guo, "Noncovalent assembly of carbon nanotube-inorganic hybrids," *Journal of Materials Chemistry*, vol. 21, no. 21, pp. 7527–7547, 2011, doi: 10.1039/c1jm10516g.
- [75] W. Yi *et al.*, "Wrapping of single-walled carbon nanotubes by a  $\pi$ -conjugated polymer: The role of polymer conformation-controlled size selectivity," *Journal of Physical Chemistry B*, vol. 112, no. 39, pp. 12263–12269, 2008, doi: 10.1021/jp804083n.
- [76] S. Shokoohi, A. Arefazar, and R. Khosrokhavar, "Silane coupling agents in polymer-based reinforced composites: A review," *Journal of Reinforced Plastics and Composites*, vol. 27, no. 5, pp. 473–485, 2008, doi: 10.1177/0731684407081391.
- [77] D. I. Tee, M. Mariatti, A. Azizan, C. H. See, and K. F. Chong, "Effect of silane-based coupling agent on the properties of silver nanoparticles filled epoxy composites," *Composites Science and Technology*, vol. 67, no. 11–12, pp. 2584–2591, 2007, doi: 10.1016/j.compscitech.2006.12.007.
- [78] F. Tan, X. Qiao, J. Chen, and H. Wang, "Effects of coupling agents on the properties of epoxy-based electrically conductive adhesives," *International Journal of Adhesion and Adhesives*, vol. 26, no. 6, pp. 406–413, 2006, doi: 10.1016/j.ijadhadh.2005.06.005.
- [79] M. W. Daniels and L. F. Francis, "Daniels W 1998," vol. 200, pp. 1–10, 1998, [Online]. Available: [papers://5744443d-a9b5-4343-acd7-0a6450d9e2a0/Paper/p13](http://papers://5744443d-a9b5-4343-acd7-0a6450d9e2a0/Paper/p13)
- [80] M. Abdelmouleh, S. Boufi, M. N. Belgacem, A. Dufresne, and A. Gandini, "Modification of cellulose fibers with functionalized silanes: Effect of the fiber treatment on the mechanical performances of cellulose-thermoset composites," *Journal of Applied Polymer Science*, vol. 98, no. 3, pp. 974–984, 2005, doi: 10.1002/app.22133.
- [81] R. Yang, Y. Liu, K. Wang, and J. Yu, "Characterization of surface interaction of inorganic fillers with silane coupling agents," *Journal of Analytical and Applied Pyrolysis*, vol. 70, no. 2, pp. 413–425, 2003, doi: 10.1016/S0165-2370(02)00200-0.
- [82] S. C. Agents, "2 2.1.," 1991.
- [83] C. Kaynak, C. Celikbilek, and G. Akovali, "Use of silane coupling agents to improve epoxy-rubber interface," *European Polymer Journal*, vol. 39, no. 6, pp. 1125–1132, 2003, doi: 10.1016/S0014-3057(02)00381-6.

- [84] A. Tezvergil, L. V. J. Lassila, A. Yli-Urpo, and P. K. Vallittu, "Repair bond strength of restorative resin composite applied to fiber-reinforced composite substrate," *Acta Odontologica Scandinavica*, vol. 62, no. 1, pp. 51–60, 2004, doi: 10.1080/00016350310008210.
- [85] M. Hashimoto, H. Takadama, M. Mizuno, and T. Kokubo, "Enhancement of mechanical strength of TiO<sub>2</sub>/high-density polyethylene composites for bone repair with silane-coupling treatment," *Materials Research Bulletin*, vol. 41, no. 3, pp. 515–524, 2006, doi: 10.1016/j.materresbull.2005.09.014.
- [86] M. Buggy, G. Bradley, and A. Sullivan, "Polymer-filler interactions in kaolin/nylon 6,6 composites containing a silane coupling agent," *Composites Part A: Applied Science and Manufacturing*, vol. 36, no. 4, pp. 437–442, 2005, doi: 10.1016/j.compositesa.2004.10.002.
- [87] P. C. Ma, J. K. Kim, and B. Z. Tang, "Functionalization of carbon nanotubes using a silane coupling agent," *Carbon*, vol. 44, no. 15, pp. 3232–3238, 2006, doi: 10.1016/j.carbon.2006.06.032.
- [88] N. M. Stark, D. J. Yelle, and U. P. Agarwal, *Techniques for Characterizing Lignin*. Elsevier Inc., 2016. doi: 10.1016/B978-0-323-35565-0.00004-7.